AN ABSTRACT OF THE THESIS OF

Abdullah Almarshad for the degree of Doctor of Philosophy in Nuclear Engineering presented on March 12, 1990.

Title: A Model for Waterside Oxidation of Zircaloy Fuel Cladding in Pressurized Water Reactors

Redacted for Privacy

Abstract approved: Andrew G. Klein

A model has been developed to predict the long-term oxidation rate of Zircaloy-4 for ex-reactor (autoclave) and in-reactor (PWR) environments and operating conditions. A computer program has been written to solve the oxygen diffusion equation by employing a fully implicit finite difference method for a one dimensional cylindrical geometry. The moving boundary of the oxide is treated by deriving a time dependent relationship to control the speed of the interface motion. New diffusion coefficients for the oxygen in the oxide film have been developed. The proposed diffusion coefficients are a function of temperature and oxygen concentration gradient in the oxide and are derived for both the pre-transition and post-transition regions.

To include the in-reactor corrosion behavior, additional factors have been considered, specifically the influence of the heat flux on the oxide-metal interface temperature, the fast neutron flux effect on the

acceleration of the corrosion rate, and the effect of the lithium hydroxide concentration on the enhancement of the corrosion rate. This model allows the prediction of the long-term oxidation weight gain and the oxide thickness on Zircaloy-4 in operating conditions which simulate the PWR conditions.

The results obtained for ex-reactor (autoclave) and in-reactor oxidation are compared with experimental data existing in the literature. The predictions are found to be in good agreement with the experimental data.

A Model For Waterside Oxidation of Zircaloy Fuel Cladding in Pressurized Water Reactors

by

Abdullah I.A. Almarshad

A THESIS

Submitted to
Oregon State University

in partial fulfillment of
the requirements for the degree of

Doctor of Philosophy

Completed March 12, 1990
Commencement June 1990

APPROVED:

Redacted for Privacy

Professor of Nuclear Engineering in charge of major

Redacted for Privacy

Head of Department of Nuclear Engineering

Redacted for Privacy

Dean of Graduate School

Date thesis is presented March 12, 1990

Typed by Sadie's Word Processing for Abdullah I. Almarshad

ACKNOWLEDGEMENT

I am deeply grateful to my advisor, Dr. Andrew C. Klein for his advice, guidance and encouragement throughout my study at Oregon State University.

Sincere appreciation is extended to the members of my doctoral committee: Dr. Alan H. Robinson, Dr. Jonathan Istok, Dr. Jose N. Reyes and Dr. William H. Warnes.

I must also acknowledge my parents and my wife for their unending support and prayers during my study and stay in the United States.

Table of Contents

List of Figures

List of Tables

A MODEL FOR WATERSIDE OXIDATION OF Zircaloy FUEL CLADDING IN PRESSURIZED WATER REACTORS

Chapter 1

Introduction

Waterside corrosion of Zircaloy has generally not been observed to be a problem under current normal pressurized water reactors (PWR) operating conditions. The uniform waterside corrosion behavior of Zircaloy-4 cladding has been highly satisfactory, and at a level in which it does not inhibit reactor operation. However, waterside corrosion of Zircaloy-4 has become an important technical issue and a subject of increased interest recently in the nuclear industry since it will become one of the limiting factors in a PWR's fuel rod performance and design. This is as a result of the industry's aims to extend the average fuel rod discharge burnups, obtain higher coolant inlet temperatures to increase the nuclear plant thermal efficiency, and to increase coolant pH and lithium concentration to reduce plant radiation levels due to corrosion products.

The purpose of this investigation is to develop a computer program model to predict long-term waterside corrosion weight gain and oxide thickness in pressurized water reactors. The proposed model can be utilized to estimate the pre- and post-transition corrosion weight gain and the oxide thickness for ex-reactor and in-reactor environments and operating conditions. The ex-reactor

simulation accounts for the effect of heat flux on the temperature at the metal-oxide interface and the increase in the oxidation rate because of the temperature gradient along the oxide layer. For in-reactor simulations other factors have been included in addition to the heat flux, such as, adding an irradiation-induced corrosion enhancement factor to account for the effect of the fast neutron fluence and a lithium hydroxide acceleration factor in order to evaluate the effect of coolant chemistry on in-reactor corrosion.

This thesis is presented in five chapters. Chapter 2 discusses the mechanism involved in the oxidation of Zircaloy and a review of the open literature available concerning both the ex- and in-reactor Zircaloy corrosion modeling. A description for the proposed model for both ex- and in-reactor simulation is included in Chapter 3, a discussion of the results is presented in Chapter 4, and Chapter 5 includes the conclusions drawn from this investigation and recommendations for further study.

Chapter 2

Literature Review of Zircaloy Oxidation

This chapter details a review of the available open literature related to the Zircaloy oxide growth mechanism and a review of the models developed to date concerning both the ex- and in-reactor Zircaloy oxidation to predict the oxide weight gain and thickness.

2.1 Zircaloy Oxidation Mechanism

In general, the corrosion behavior of Zircaloy starts with an adherent thin black oxide film and proceeds with a simple cubic rate equation. It is then followed by a transition to a gray or white oxide with linear rate equation. This behavior is often presented graphically as weight gain versus exposure time, as shown schematically in Figure (2.1)[1] The first period is called the pre-transition growth regime. Once the oxide reaches a critical thickness (transition or breakaway), the second period begins which is called the post-transition growth regime, where the corrosion rate sharply increases due to the formation of pores and cracks in the oxide film structure, allowing more oxygen to diffuse towards the oxide-metal interface. A close inspection of the oxide shows a variety of structures, depending upon the temperature attained and

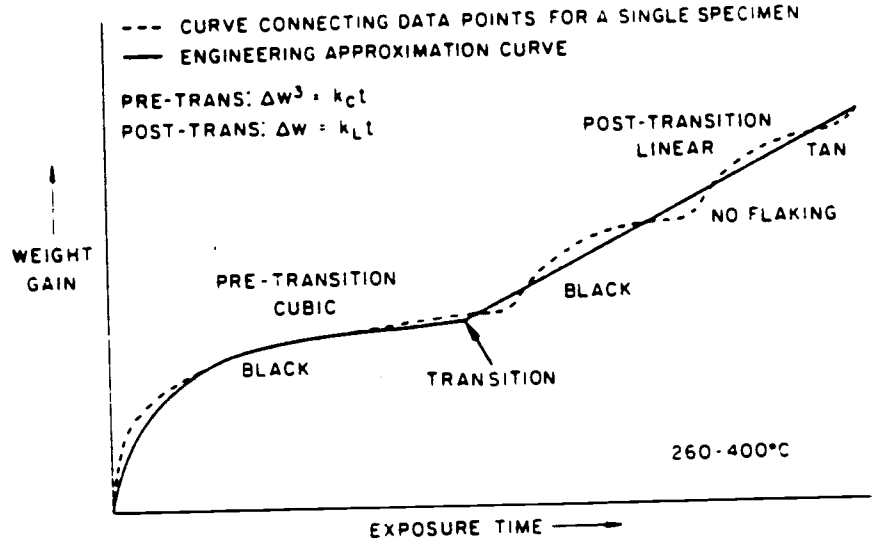

Figure 2.1 Schematic representation of corrosion of Zircaloy-2 and Zircaloy-4 in the temperature range 260 to 400 °C[1].

the oxygen concentration. At temperatures below 1144°K (871°C) two main material structures are present, an outer layer of zirconia adjacent to a layer of alpha-Zr which contains oxygen in solid solution. At temperatures above 1255 °K (982°C) at least three layers can be easily identified: an external zirconia layer, an intermediate "oxygen stabilized" alpha layer, and an inner layer of base metal comprised of transformed beta zirconium[2].

Parfenov, et al.[3] introduced a mechanism which describes the oxidation of Zircaloy in water and steam. The overall oxidation reaction can be represented as two separate reactions occurring simulatenously. First, the interaction of an anionic vacancy and two electrons with a molecule of water at the oxide-corrosive medium interface leads to the formation of an oxygen ion and two hydrogen ions:

$$\square^{++} + 2e + H_2O \text{ -----> } O^{--} + 2H^{+} \qquad (2.1)$$

where: $\square^{++}$ is an anionic vacancy in the oxide lattice,

2e two free electrons formed at the oxide-metal interface, and

O^{--} oxygen ion formed at the water-oxide interface.

Second, an oxygen ion diffuses through the oxide film to the metal and reacts with a zirconium atom on the oxide-metal interface, forming a molecule of zirconium dioxide, an anionic vacancy, and two free electrons:

$$2O^{--} + Zr \text{ -----> } ZrO_2 + 2e + \square^{++} \qquad (2.2)$$

The anionic vacancies and the free electrons diffuse to the oxide-corrosive medium interface. Thus, a constant gradient of vacancies and oxygen ions is maintained. The oxidation proceeds continuously as a result of the inward diffusion of oxygen to the metal, and it is this diffusion which is the rate-limiting step in the oxidation process.

2.2 Zircaloy Oxidation Models Review

A literature review of Zircaloy oxidation modeling is presented. Two approaches have been employed, the first approach is by deriving an analytical solution to the basic diffusion equations for a one-dimensional slab geometry. This type of solution has been utilized for short-term and high temperature oxidation under transient conditions such as a loss-of-coolant accident (LOCA), where several phases are present simultaneously and phase transformations take place. In addition, high temperature transient oxidation correlations, such as those acceptable to the U.S. Nuclear Regulatory Commission (e.g.: that developed by Cathcart[4]), have been developed. Unfortunately these correlations are of limited application in long-term oxidation studies because they were obtained for a temperature range between 900 and 1500°C. The second approach is by generating an

empirical relation from experimental data to simulate the long-term ex-reactor and in-reactor corrosion kinetics.

2.2.1 Analytical Solutions

High temperature oxidation of Zircaloys has been extensively studied by several investigators, and different analytical solutions have been proposed to determine the oxide thickness and the oxygen concentration through the oxide and other phases, such as alpha and beta, according to the oxygen concentration and Zircaloy temperature.

The basic mathematical approach used to obtain the analytical solution to the diffusion equations under different initial and boundary conditions as described and the assumptions can be found in the technical literature describing the corrosion of Zircaloy-2 and -4 in hot water and steam. Wagner's methods for moving boundary problems are outlined by Jost[5] were utilized by Pemsler,[6] Rosa,[7] Pawel,[8] Dollins,[9] and Garcia[10] in a number of papers related to the oxidation of the Zircaloy.

The following are Wagner's equations for calculating the gas concentration which has diffused into a finite slab under isothermal conditions. The diffusion coefficients are obtained experimentally and are independent of the concentration. The oxygen diffusion equations for two phase configuration, the oxide (phase I) and the underlaying Zircaloy alpha phase (phase II) separated by a

moving oxide-metal interface as shown in Figure (2.2) are given by:

$$\text{Phase I:} \quad \frac{\partial C_I(x,t)}{\partial t} = D_I \frac{\partial^2 C(x,t)}{\partial x^2} \qquad \text{for } 0 < x < \xi \qquad (2.3)$$

$$\text{Phase II:} \quad \frac{\partial C_{II}(x,t)}{\partial t} = D_{II} \frac{\partial^2 C(x,t)}{\partial x^2} \qquad \text{for } x > \xi \qquad (2.4)$$

and

$$D_I = D_{I0} \exp(-E_I/RT) \qquad (2.5)$$

$$D_{II} = D_{II0} \exp(-E_{II}/RT) \qquad (2.6)$$

where D_I is the diffusion coefficient in the oxide (phase I), cm^2/sec,

D_{II} is the diffusion cosfficient in the Zircaloy-alpha phase (phase II), cm^2/sec,

D_{I0} and D_{II0} are constants, cm^2/sec,

E_I is the activation energy for diffusion in the oxide, cal/mole,

E_{II} is the activation energy for diffusion in the Zircaloy alpha, cal/mole,

R is the gas constant, cal/K-mol, and

T is the absolute temperature, K

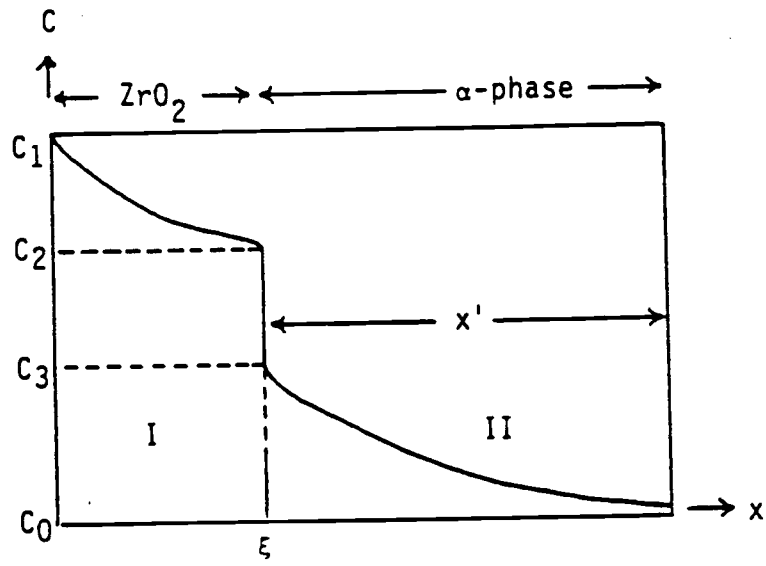

Figure 2.2. Schematic diagram of a system with two solid phases I (oxide) and II (Zr-α phase).

ξ : Moving interface distance from the outer surface.

C_0: Initial oxygen concentration uniformly distributed in the solid.

C_1: Equilibrium concentration of oxygen in gas-phase I.

C_2: Equilibrium concentration of oxygen at phase I - phase II interface - phase I side.

C_3: Equilibrium concentration of oxygen at phase I - phase II interface - phase II side.

The initial condition at time zero where the oxygen concentration is equal to the initial concentration in the Zircaloy before the oxidation takes phase can be written as:

$$C = C_0 \quad \text{at } x > 0 \quad \text{and} \quad t = 0 \tag{2.7}$$

The boundary conditions are:

$$C = C_1 \text{ at } x = 0 \quad \text{and} \quad t > 0 \tag{2.8}$$
$$C = C_2 \text{ at } x = \xi_{-0} \qquad \text{phase I} \tag{2.9}$$
$$C = C_3 \text{ at } x = \xi_{+0} \qquad \text{phase II} \tag{2.10}$$

At the plane of discontinuity, $x = \xi$, the approximate relation for the amount of diffusing substance in $d\xi$ displacement is given by:

$$(C_2 - C_3)\, d\xi = -D_I\left(\frac{\partial C}{\partial x}\right)_{\xi-0} + D_{II}\left(\frac{\partial C}{\partial x}\right)_{\xi+0} \tag{2.11}$$

The particular integral for phase I, satisfying the initial condition is:

$$C(x,t) = C_1 - B_I \operatorname{erf}\left(\frac{x}{2\sqrt{D_I t}}\right) \qquad \text{for } 0 < x < \xi \tag{2.12}$$

Where $$B_I = C_1 - C_2(\infty) \tag{2.13}$$

A particular integral for phase II, satisfying the boundary condition (2.8) is:

$$C(x,t) = C_0 - B_{II}\left[1 - \operatorname{erf}\left(\frac{x}{2\sqrt{D_{II} t}}\right)\right] \qquad \text{for } x > \xi \tag{2.14}$$

where $$B_{II} = C_3 - C_0(\infty) \tag{2.15}$$

Wagner has shown that for a unidirectional diffusion process, the displacement of the oxide-metal interface can be expressed as:

$$\xi = 2\gamma\sqrt{D_I t} \tag{2.16}$$

where γ is a proportionality constant.

The oxygen concentration at the moving interface for both phases can be obtained by substituting equations (2.12), (2.14) and (2.16) in equations (2.9), (2.10) and (2.11).

$$C_2 = C_1 - B_I \ \text{erf}(\gamma) \tag{2.17}$$

$$C_3 = C_0 - B_{II} \ [1 - \text{erf} \ (\gamma \ \phi)] \tag{2.18}$$

and

$$C_2 - C_3 = \frac{B_I}{\sqrt{\pi}\gamma} \exp(-\gamma^2) - \frac{B_{II}}{\gamma\sqrt{\pi}\sqrt{\phi}} \exp(-\gamma^2\phi) \tag{2.19}$$

where ϕ is the ratio of the diffusion coefficients

$$\phi = \frac{D_I}{D_{II}} \tag{2.20}$$

Finally, by eliminating B_I and B_{II} from equations

$$C_2 - C_3 = \frac{C_1 - C_2}{\sqrt{\pi}\ \gamma \text{erf}\gamma} \exp(-\gamma^2) - \frac{C_3 - C_0}{\sqrt{\pi\phi}\ \gamma\,[1-\text{erf}(\gamma\sqrt{\phi}\ )]} \exp(-\gamma^2) \tag{2.21}$$

and

$$C_1 - C_2 = \frac{C_2 - C_3}{\exp(-\gamma^2)} \sqrt{\pi}\ \gamma \text{erf}\gamma + \frac{C_3 - C_0}{\sqrt{\pi\phi}\ \gamma\,[1-\text{erf}(\gamma\sqrt{\phi}\ )]} \exp(-\gamma^2) \tag{2.22}$$

From equation (2.21) γ can be evaluated by numerical or graphical methods if the diffusion coefficients and the concentrations are known.

Pemsler[6] evaluated the amount and gradient of oxygen in the metal substrate beneath the oxide film by utilizing Wagner's solution and by accounting for the volume expansion which is related to the metal-to-oxide transformation and is associated with oxygen dissolved in the α-phase. The solution to this problem for the case of zirconium oxidizing at a parabolic rate is given by solving for the oxygen concentration, C, at a distance x' from the oxide/metal interface:[11]

$$C = C_3 \frac{\operatorname{erfc}\left\{(x'/2\sqrt{D_{11}t}) + \left(\frac{V_{Zr}}{V_{ZrO_2}}\right)\left(\sqrt{\frac{k'}{D_{11}}}\right)\right\}}{\operatorname{erfc}\left\{\left(\frac{V_{Zr}}{V_{ZrO_2}}\right)\left(\sqrt{\frac{k'}{D_{11}}}\right)\right\}} \tag{2.23}$$

where C_3 is the oxygen concentration in zirconium coexisting with ZrO_2, V_{Zr} is the molar volume of zirconium, V_{ZrO_2} is the molar volume of zirconium oxide, and k' is the parabolic rate constant. The ratio of ZrO_2 molar volume to the Zr molar volume is called the Pilling-Bedworth factor,

$$P = \frac{V_{ZrO_2}}{V_{Zr}} \tag{2.24}$$

The molecular volume (molar volume) is defined by the volume occupied by 1 mole.[12]

$$\text{molar volume} = \frac{\text{molecular weight}}{\text{density}} \quad \text{cm}^3 \tag{2.25}$$

$$\text{For } ZrO_2 \text{ the molar volume} = \frac{123.22}{5.89} = 22.0 \text{ cm}^3. \tag{2.26}$$

$$\text{For Zr the molar volume} = \frac{91.22}{6.49} = 14.1 \text{ cm}^3. \tag{2.27}$$

Equation (2.23) may be rewritten as:

$$C = C_3 \frac{\operatorname{erfc}\left(\frac{x}{2\sqrt{D_{II}t}}\right)}{\operatorname{erfc}\left(\frac{\xi}{2\sqrt{D_{II}t}}\right)} \tag{2.28}$$

where $x = \xi + x'$ (2.29)

Integration of equation (2.28) gives the total amount of oxygen present in the metal beneath the oxide film.

$$W_{II} = 2C_3\sqrt{D_{II}t}\left(\frac{\exp(-\xi/4D_{II}t)}{\sqrt{\pi}\ \operatorname{erfc}(\xi/2\sqrt{D_{II}t})} - \frac{\xi}{2\sqrt{D_{II}t}}\right) \tag{2.30}$$

where W_{II} is the quantity of oxygen dissolved in the metal per unit area of surface.

The solution of Wagner's equations in the case of a semi-infinite solid with and without considering the volume expansion of the metal to the oxide ratio has been presented by Denis and Garcia[13] in a series of papers related to the oxidation of Zircaloy.

In the case of no volume expansion the concentrations are found to be:

$$C_I(x,t) = C_1 - \frac{C_1 - C_2}{\operatorname{erf}(\gamma)} \operatorname{erf}\left(\frac{x}{2\sqrt{D_I t}}\right) \qquad \text{for } 0 < x < \xi \tag{2.31}$$

$$C_{II}(x,t) = C_3 \frac{\operatorname{erfc}\left(\frac{x}{2\sqrt{D_{II}t}}\right)}{\operatorname{erfc}(\gamma\sqrt{\phi})} \qquad \text{for } x < \xi \tag{2.32}$$

where ϕ is the ratio of the diffusion coefficients.

$$\phi = \frac{D_I}{D_{II}} \tag{2.33}$$

and

$$\gamma = \frac{C_1 - C_2}{C_2 - C_3} \frac{\exp(-\gamma^2)}{\sqrt{\phi}\ \mathrm{erf}(\gamma)} - \frac{C_3}{C_2 - C_3} \frac{\exp(-\gamma\sqrt{\phi})^2}{\sqrt{\pi\phi}\ \mathrm{erfc}(\gamma\sqrt{\phi})} \tag{2.34}$$

Therefore the gas mass per unit area in phase I and phase II can be determined by integrating the functions $C_I(x,t)$ and $C_{II}(x,t)$ over their respective intervals of validity to give:

$$W_I = 2\sqrt{D_I}\left[C_2\gamma - \frac{C_1 - C_2}{\sqrt{\pi}\ \mathrm{erf}(\gamma)}\left[\exp(-\gamma^2) - 1\right]\right]\sqrt{t} \tag{2.35}$$

$$W_{II} = 2\sqrt{D_{II}}\, C_3\left[\frac{\exp[-(\gamma\sqrt{\phi})^2]}{\sqrt{\pi}\ \mathrm{erfc}(\gamma\sqrt{\phi})} - \gamma\sqrt{\phi}\right]\sqrt{t} \tag{2.36}$$

and then the total mass of gas per unit area in the two phases is found to be:

$$W_T = W_I + W_{II} \tag{2.37}$$

To account for the effect of the temperature change during temperature transients, Garcia[14] modified the isothermal diffusion coefficients to be time dependent with a linear increase of temperature with time. The analytical equations necessary for a temperature transient corresponding to the system of Figure (2.2) can be expressed as follow:

$$\frac{\partial C_I(x,t)}{\partial T} = D_I(t)\frac{\partial^2 C_I(x,t)}{\partial x^2} \tag{2.38}$$

$$\frac{\partial C_{II}(x,t)}{\partial t} = D_{II}(t) \frac{\partial^2 C_{II}(x,t)}{\partial x^2} \tag{2.39}$$

and the interface velocity at the instant t:

$$\frac{\partial \xi}{dt} = -\frac{D_I(t)}{C_2 - C_3}\left[\frac{\partial C_I}{\partial x}\right]_\epsilon + \frac{D_{II}(t)}{C_2 - C_3}\left[\frac{\partial C_{II}}{\partial x}\right]_\epsilon \tag{2.40}$$

The following transformation is introduced:

$$ds = D_I(t)\, dt \tag{2.41}$$

and defining

$$\phi = \frac{D_I(t)}{D_{II}(t)} \tag{2.42}$$

Equation (2.38) and (2.39) in terms of the new variables, become:

$$\frac{\partial C_I}{\partial s} = \frac{\partial^2 C_I}{\partial x^2} \tag{2.43}$$

$$\frac{\partial C_{II}}{\partial s} = \frac{1}{\phi}\frac{\partial C_{II}}{\partial x^2} \tag{2.44}$$

Similarly, equation (2.4) becomes:

$$\frac{\partial \xi}{\partial s} = \frac{1}{C_2 - C_3}\left[\frac{\partial C_I}{\partial x}\right]_\epsilon + \frac{1}{\phi(C_2 - C_3)}\left[\frac{\partial C_{II}}{\partial x}\right]_\epsilon \tag{2.45}$$

and the diffusion coefficients are expressed by:

$$D_I(t) = D_{I0} \exp\,[-E_I/RT(t)] \tag{2.46}$$

$$D_{II}(t) = D_{II0} \exp\,[-E_{II}/RT(t)] \tag{2.47}$$

Thus equation (2.42) may be written as

$$\phi = \frac{D_{I0}}{D_{II0}} \exp\left[-(E_I - E_{II})/RT(t)\right] \tag{2.48}$$

for the simple case where the activation energy (E) in the gaseous element diffusion is to be the same for every phase.

$$E_I = E_{II} = E \tag{2.49}$$

Therefore equation 2.48 becomes:

$$\phi = \frac{D_{I0}}{D_{II0}} \tag{2.50}$$

The solution for the gas concentration in phase I and phase II is then:

$$C_I(x,s) = C_I - \frac{C_I - C_2}{\operatorname{erf}(\gamma)} \operatorname{erf}\left(\frac{x}{2\sqrt{s}}\right) \qquad \text{for } 0 < x < \xi \tag{2.51}$$

$$C_{II}(x,s) = \frac{C_3}{\operatorname{erfc}(\gamma\sqrt{\phi})} \operatorname{erfc}\left(\frac{x}{2}\sqrt{\phi/s}\right) \qquad \text{for } \xi < x < \infty \tag{2.52}$$

The following expression results for γ:

$$\gamma = \frac{C_1 - C_2}{C_2 - C_3} \frac{\exp(-\gamma^2)}{\sqrt{\pi}\operatorname{erf}(\gamma)} - \frac{C_2}{C_2 - C_3} \frac{\exp(-\gamma\sqrt{\phi})^2}{\sqrt{\pi\phi}\operatorname{erfc}(\gamma\sqrt{\phi})} \tag{2.53}$$

where

$$C_I(\xi,s) = C_2 \qquad \text{at } x = \xi \tag{2.54}$$

$$C_{II}(\xi,s) = C_3 \qquad \text{at } x = \xi \tag{2.55}$$

thus

$$\xi = 2\gamma\sqrt{s} \tag{2.56}$$

and remembering that this analysis is derived for a fast transient such as a LOCA, the interface displacement is driven by choosing a temperature transient varying linearly with time of the form

$$T(t) = at + b \tag{2.57}$$

and then in this particular case, the location of the boundary is found to be:

$$\xi = 2\gamma \left[\frac{D_{10}E}{aR}\right]^{1/2} \left[\frac{E_2\left(\frac{E}{R(at+b)}\right)}{\frac{E}{R(at+b)}} - \frac{E_2\left(\frac{E}{Rb}\right)}{\frac{E}{Rb}}\right]^{1/2} \tag{2.58}$$

where $E_2(Z)$ is the second order exponential integral function.

A more realistic treatment for the change in density between the metal and the oxide due to the presence of pores and cracks was introduced by Denis and Garcia[13]. The solution for the diffusion equations for the two phase system is described by two approaches: (I) with the co-ordinate origin fixed to the gas-solid interface and (II) with the co-ordinate system fixed to the metal as shown in Figure (2.3).

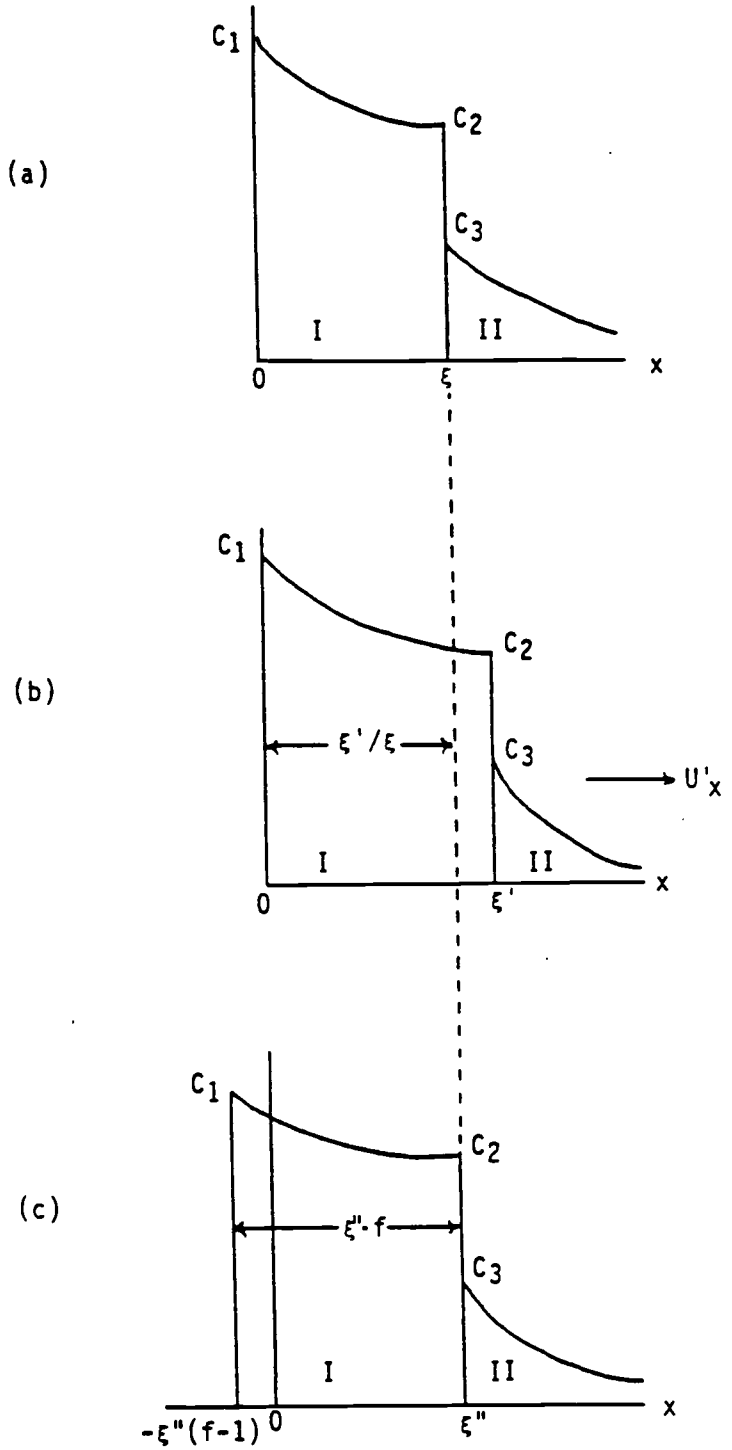

Figure 2.3 Schematic diagram of a system with two solid phases separated by a moving interface, (a) constant metallic atom density in both solid phases, (b) variable metallic atom density and coordinate system origin fixed at the gas-solid interface, (c) variable metallic atom density and coordinate system fixed to phase II.

In the previous approaches the oxide-metal interface displaces a distance $d\xi$ during dt, but if the solvent density change is considered, the oxide thickness increases $f \cdot d\xi$ in the same dt where f represents the relation between the oxide thickness and that of the original metal. In other words, f is the oxide expansion coefficient.

I. Co-ordinate Origin Fixed to the Gas-Solid Interface

In this co-ordinate system the oxide density change gives rise to a rigid displacement dx of phase II during dt, as may be seen in Figure (2.3b). In this discussion, then

$$dx = d\xi' - d\xi \tag{2.59}$$

where $d\xi' = f \cdot d\xi$ is the oxide thickness generated from oxidation of a metal layer of thickness $d\xi$. The phase II displacement rate in the +x direction is then:

$$u_x' = \frac{dx}{dt} = \frac{d\xi'}{dt}\left(1 - \frac{1}{f}\right) \tag{2.60}$$

The diffusion equations become:

$$\frac{\partial C_I}{\partial t} = D_I \frac{\partial^2 C_I}{\partial x^2} \tag{2.61}$$

and

$$\frac{\partial C_{II}}{\partial t} = D_{II} \frac{\partial^2 C_{II}}{\partial x^2} - u_x' \frac{\partial C_{II}}{\partial x} \tag{2.62}$$

The gas concentration in both phases is then found to be:

$$C_I(x,t) = C_1 \frac{C_1 - C_2}{\operatorname{erf}\gamma'} \operatorname{erf}\left(\frac{x}{2\sqrt{D_1 t}}\right) \qquad \text{for } 0 < x < \xi' \tag{2.63}$$

and

$$C_{II}(x,t) = C_3 \frac{\operatorname{erfc}\left[\frac{x}{2\sqrt{D_1 t}}\right] - \gamma'\sqrt{\phi}\left(1-\frac{1}{f}\right)}{\operatorname{erfc}\left[\gamma'\sqrt{\frac{\phi}{f}}\right]} \quad \text{for } x > \xi' \tag{2.64}$$

with

$$\gamma' = \frac{C_1 - C_2}{C_2' - C_3}\frac{\exp(-\gamma'^2)}{\sqrt{\pi}\,\operatorname{erf}\gamma'} - \frac{C_3}{C_2' - C_3}\frac{\exp\left[-\left(\gamma'\sqrt{\frac{\pi}{f}}\right)^2\right]}{\sqrt{\pi\phi}\,\operatorname{erfc}\left[\gamma'\sqrt{\frac{\phi}{f}}\right]} \tag{2.65}$$

and

$$\xi = 2\gamma'\sqrt{D_1 t} \tag{2.66}$$

$$W_I = 2\sqrt{D_I}\left[C_2\gamma' - \frac{C_1 - C_2}{\sqrt{\pi}\,\operatorname{erf}\gamma'}\left[\exp(-\gamma'^2) - 1\right]\right] \tag{2.67}$$

$$W_{II} = 2\sqrt{D_{II}}\,C_3\left[\frac{\exp\left[-\left(\gamma'\sqrt{\frac{\phi}{f}}\right)^2\right]}{\sqrt{\pi}\,\operatorname{erfc}\left[\gamma'\sqrt{\frac{\phi}{f}}\right]} - \frac{\gamma'\sqrt{\phi}}{f}\right] \tag{2.68}$$

II. Co-ordinate System Fixed to Phase II

If the problem is described from a co-ordinate system fixed to phase II, with its origin in the original gas-solid interface (Figure 2.3c), the interface I-II displacement $d\xi''$ will produce a rigid movement of the oxide in the -x direction by:

$$dx = -(f \cdot d\xi'' - d\xi'') = -d\xi''(f - 1) \tag{2.69}$$

where $f \cdot d\xi''$ is the oxide thickness generated from a $d\xi''$ metal thickness. The displacement rate is:

$$u_x'' = \frac{dx}{dt} = -\frac{d\xi''}{dt}(f-1) \tag{2.70}$$

The diffusion equations become:

$$\frac{\partial C_I}{\partial t} = D_I \frac{\partial^2 C_I}{\partial x^2} - u_x'' \frac{\partial C_I}{\partial x} \tag{2.71}$$

$$\frac{\partial C_{II}}{\partial t} = D_{II} \frac{\partial^2 C_{II}}{\partial x^2} \tag{2.72}$$

and their solutions are:

$$C_I(x,t) = C_1 \frac{C_1 - C_2}{\operatorname{erf}(\gamma'' f)} \operatorname{erf}\left[\frac{x}{2\sqrt{D_I t}} + \gamma''(f-1)\right] \quad \text{for } -\xi''(f-1) < x < \xi'' \tag{2.73}$$

and

$$C_{II}(x,t) = C_3 \frac{\operatorname{erfc}\left[\frac{x\sqrt{\phi}}{2\sqrt{D_I t}}\right]}{\operatorname{erfc}(\gamma''\sqrt{\phi})} \quad \text{for } x \geq \xi'' \tag{2.74}$$

with

$$\xi'' = 2\gamma''\sqrt{D_I t} \tag{2.75}$$

$$\gamma'' = \frac{C_1 - C_2}{C_2'' - C_3} \frac{\exp[-(\gamma'' f)^2]}{\sqrt{\pi}\operatorname{erf}(\gamma'' f)} - \frac{C_3}{C_2'' - C_3} \frac{\exp[-(\gamma''\sqrt{\phi})^2]}{\sqrt{\pi\phi}\operatorname{erfc}(\gamma''\sqrt{\phi})} \tag{2.76}$$

$$W_I = 2\sqrt{D_I}\left[C_2\gamma'' f - \frac{C_1 - C_2}{\sqrt{\pi}\operatorname{erf}(\gamma'' f)} \exp[-(\gamma'' f)^2] - 1\right] \tag{2.77}$$

$$W_{II} = 2\sqrt{D_{II}} C_3 \left[\frac{\exp[-(\gamma''\sqrt{\phi})^2]}{\sqrt{\pi}\operatorname{erfc}(\gamma''\sqrt{\phi})} - \gamma''\sqrt{\phi}\right] \tag{2.78}$$

$$W_T = W_I + W_{II} \tag{2.79}$$

The actual oxide expansion coefficient, f, is the product of two expansion coefficients: the expansion coefficient f_0 owing to the metal-oxide phase change, and the expansion coefficient f_p owing to pores and cracks in the oxide. The overall oxide expansion coefficient is then given as:

$$f = f_0 \cdot f_p \tag{2.80}$$

When the oxide density is less than the metal density it becomes important to consider the different cases which relate to the metal/oxide phase change expansion coefficient, f_0, to the Pilling-Bedworth factor, P. This results in three limiting cases for the expansion coefficient:

(a) The oxide expansion is completely anisotropic in such a way that an increase in volume only implies an increase of the oxide layer thickness and the oxide to metal volume ratio remains equal to 1. In this case $P = f_0$ and no stresses appear in the oxide-metal interface.

(b) The oxide expansion is isotropic, so that the expansion takes place in the three dimensions equally and generates interface stresses: i.e., compression in the oxide and tension in the metal oxide, and $P = f_0^3$.

(c) It is also possible to assume such an anisotropic expansion that the oxide thickness remains equal to that of the original metal.

Besides the above described expansion coefficient, an increase in the oxide volume is produced due to the formation of pores and cracks. The coefficient which describes this effect, f_p, has a minimum value equal to 1.

In both coordinate systems it is found that

$f \geq 1$ and $P \geq 1$

and by considering the volume of the pores and cracks, the Pilling-Bedworth factor becomes

$$P_p = \frac{V_{ZrO_2}+P}{V_{ZrO_2}} \tag{2.81}$$

and the modified total Pilling-Bedworth factor becomes:

$$P_T = P(P_p) = \frac{V_{ZrO_2}}{V_{Zr}} \frac{V_{ZrO_2}+P}{V_{ZrO_2}} \tag{2.82}$$

As in the previous analysis, limiting cases for the expansion due to pores and cracks formation may be considered:

(a) the oxide volume increases due to pores and cracks in the oxide thickness direction but the oxide area is constant and thus the expansion is anisotropic and $f_p = P_p$,

(b) the case of isotropic expansion yields $P_p = f_p^3$, and

(c) if the formation of pores and cracks only modifies the oxide area in contact with the metal but not its thickness, $f_p = 1$.

Reference 12 lists all the possible combinations between the cases of f_0 and f_p. However, because the pores and

cracks formation are time and temperature dependent processes, an experimental correlation may be needed to determine f_p in order to obtain a more accurate expansion coefficient.

2.2.2 Ex-Reactor Empirical Models

Several models have been created to simulate ex-reactor (autoclave) long-term oxidation based on experimental data. The models vary depending on the data used in the analysis, however, there are some factors which may influence the corrosion behavior and the weight gain prediction from one model to another such as, the specimens' composition, surface treatment, and heat treatment.

The influence of the composition of Zircaloy - type alloys in autoclave tests has been evaluated by Eucken, et al.[15] with respect to uniform corrosion. A variety of ingots with different compositions were tested, the alloy elements covered the following ranges: tin: 0.2 to 1.7%; iron: 0.05 to 0.53%; chromium: 0.04 to 1.05%; and nickel: 0.003 to 0.046%. In addition, oxygen, carbon, silicon, and phosphorous were varied over the range of standard Zircaloy contents. For example, their results show that at 350 °C and 400 °C the time to transition from the cubic to linear rate increases and the post-transition rate decreases with decreasing tin and carbon and increasing silicon content. Figure (2.4) and (2.5) show the effect of increasing the

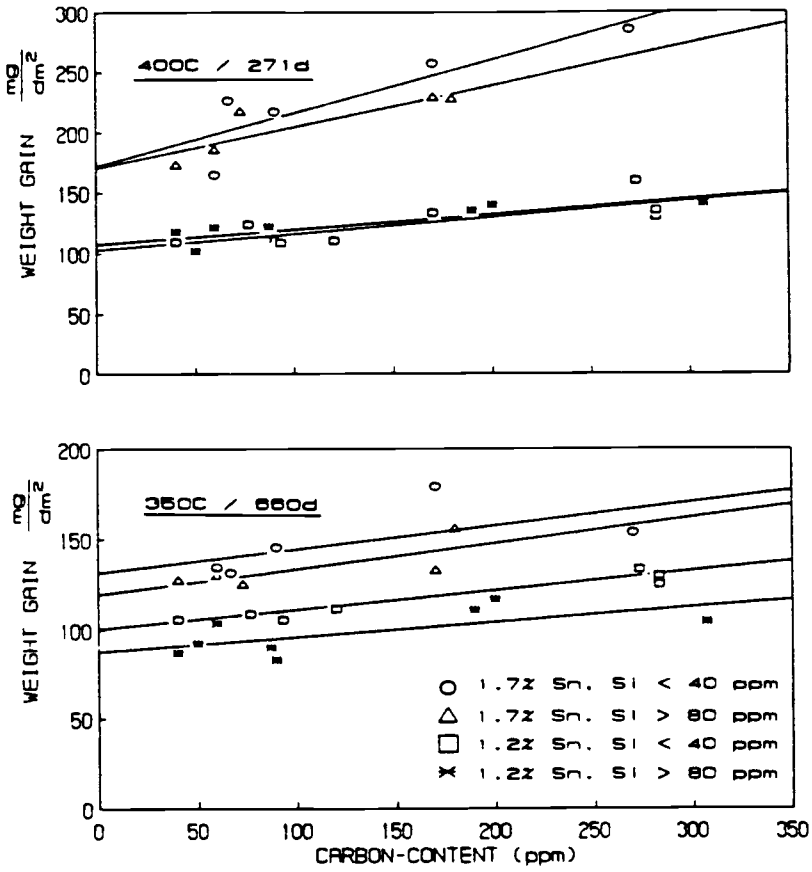

Figure 2.4 Effect of carbon, tin and silicon on ex-reactor corrosion at 350 °C and 400 °C,[15].

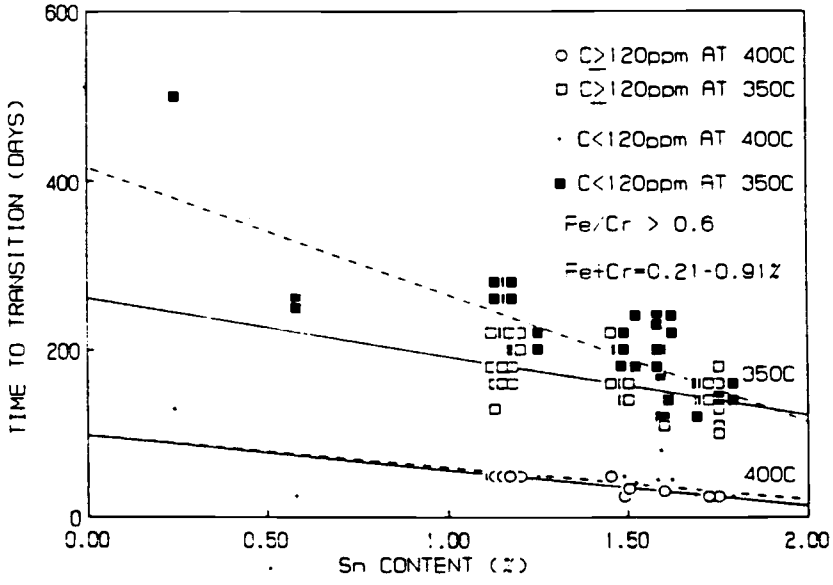

Figure 2.5 Effect of tin content on time to transition[15].

content of tin, carbon and silicon on the weight gain and time to transition.

The oxidation kinetics of 0.5 wt% binary alloys of iron, nickel, and chromium in Zirconium were studied by Ploc[16] for several surface preparations. Figure (2.6) shows the influence of the alloy surface preparation which revealed that the precipitates at the free surface caused oxide cracking, which in turn led to accelerated oxidation. That the acceleration was due to cracking induced by the local surface geometry was confirmed by the observation that smooth alloy surfaces reduced oxidation rates.

Heat treatment is also one of the factors affecting the corrosion resistance of Zirconium and Zirconium alloys, by influencing the properties of the oxide film formed on the surface. Wadman and Andren[17] made a study for two different Zircaloy-4 fuel cladding materials which had approximately the same composition, but they were exposed to different heat treatment conditions. The tests were carried out by means of autoclave test facility. Results of the autoclave tests are shown in Figure (2.7).

It can be seen that Material A, with longer annealing times at higher temperature has considerably higher uniform corrosion resistance than the experimental Material B. This difference in the oxidation rate is explained in terms of iron diffusion to the precipitates during final

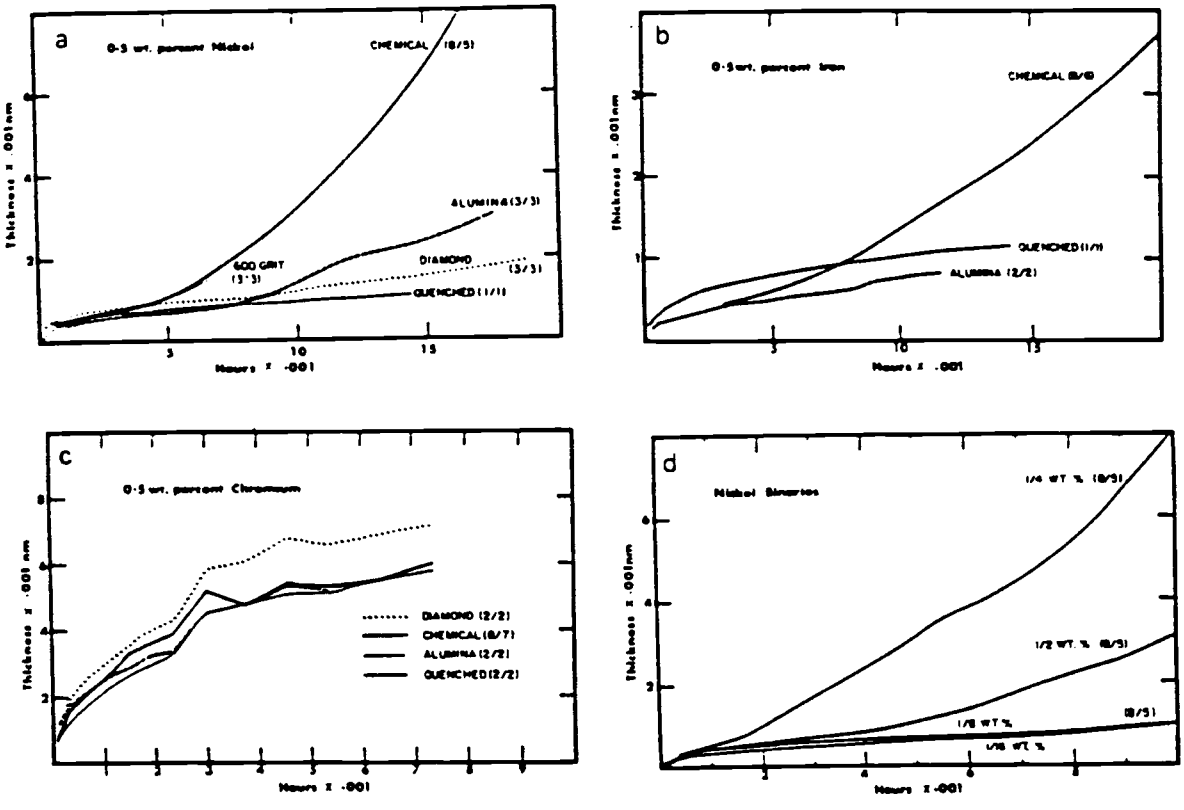

Figure 2.6 The influence of the alloy surface preparation on the oxidation of the 0.5 wt% binaries: (a) nickel, (b) iron, (c) chromium, and (d) variation of nickel content (chemically polished), numbers in brackets indicate the number of specimens at the beginning and end of the tests, respectively[16].

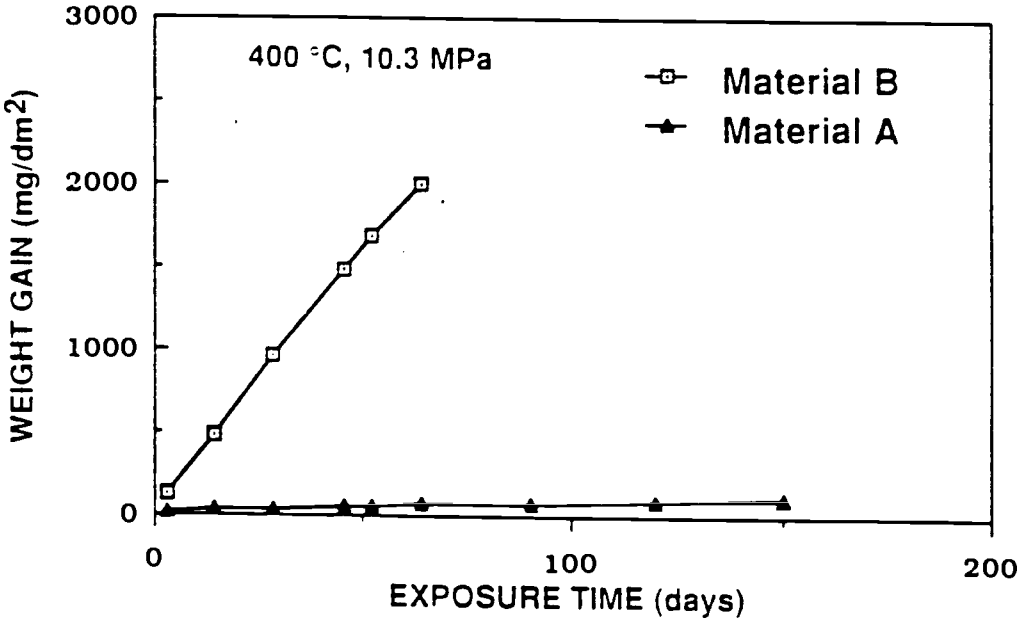

Figure 2.7 Static autoclave corrosion test in steam at 400 °C and 10.3 MPa of the two materials studied[17].

annealing so the material with higher iron concentration in the matrix showed the best uniform corrosion properties.

2.2.2.1 Hillner Model

Hillner[1] compiled Zircaloy-2 and -4 data from nine references into a single isothermal corrosion curve. The Hillner model is one of the standard isothermal models upon which other authors based their models. It was assumed that the pre-transition corrosion kinetics were cubic and the post-transition are assumed to be linear with respect to time. Values of K_c and K_l, the cubic and linear constants, were determined from the compiled data, and yielded the following empirical relationships:

In the pre-transition region the weight gain is found to be:

$$\Delta W^3 = 6.36 \times 10^{11} \exp [-13636/T] \times t \qquad (2.83)$$

Post-transition weight gain is given by:

$$\Delta W = 1.12 \times 10^{8} \exp [-12529/T] \times t \qquad (2.84)$$

where ΔW is the weight gain (mg/dm^2),

T is the absolute temperature (°K), and

t is the total exposure time in days

These expressions are valid in the temperature range from 533°K to 673°K. The weight gain and time to transition can be calculated by solving equation (2.83) and (2.84) to have:

$$\Delta W_t = 7.53 \times 10 \exp [-553.6/T] \qquad (2.85)$$

$$t_t = 6.73 \times 10^{-7} \exp [11975/T] \quad (2.86)$$

2.2.2.2 Van der Linde Model

The Van der Linde[18] model is a set of empirical relations describing Zircaloy isothermal corrosion, and is also based on ex-reactor data.

In the pre-transition region the weight gain is found to be:

$$\Delta W^3 = 1.99 \times 10^{13} \exp [-31116/RT] \, xt \quad (2.87)$$

Post-transition weight gain is given by:

$$\Delta W = \Delta W_t + 23.0 \times 10^8 \exp [-28613/RT] \times (t-t_t) \quad (2.88)$$

The weight gain, ΔW_t and time t_t at transition are then given as:

$$\Delta W_t = 1.23 \times 10^2 \exp [-1570/RT] \quad (2.89)$$

$$t_t = 9.30 \times 10^{-8} \exp [2642/RT] \quad (2.90)$$

2.2.2.3 Dyce Model

Dyce's correlations[18] are derived for the isothermal corrosion kinetics of Zircaloys and they are similar to Van der Linde correlations, however the constants are different.

In the pre-transition region the weight gain is found to be:

$$\Delta W^3 = 5.07 \times 10^{13} \exp [-32289/RT] \times t \quad (2.91)$$

Post-transition weight gain is given by:

$$\Delta W = \Delta W_t + 6.53 \times 10^9 \exp [-29915/RT] \times (t-t_t) \quad (2.92)$$

2.2.2.4 Dalgaard Model

Dalgaard's model[18] has the same typical form as given above, however the pre-transition period is neglected.

$$\Delta W = 1.84 \times 10^7 \exp [-22200/RT] \times t \quad (2.93)$$

2.2.3 In-Reactor Empirical Models

The in-reactor corrosion behavior of the Zircaloy is different from the ex-reactor behavior. Several additional factors must be considered for long-term in-reactor oxidation modeling such as, the effect of the heat flux and the fast neutron flux, the coolant chemistry and the power history. Most of the available models have been created using data from ex-reactor (autoclave) testing, and are then extrapolated to reactor conditions. A review of the published in-reactor corrosion models is presented below.

2.2.3.1 Chort Model

The Chort model[19] was developed to account for the observed weight gain differences between SRA (stress-relief annealed) and RXA (recrystallized annealed) Zircaloy-4 tubing in the post-transition region. This model is based on the work of Bryner[20], who showed that Zircaloy corrodes cyclically in high temperature water. The thermal corro-

sion weight which considers the heat flux effect, can be calculated by using the following equations:

$$W_{TH} = [A \exp(-Q/T) \times t]^{1/3} \quad (2.94)$$

where W_{TH} is the thermal corrosion weight gain/unit area,

A is a fitting constant for thermal corrosion,

Q is the activation energy for thermal corrosion,

T is the cladding surface temperature, and

t is the exposure time

Chort accounts for the acceleration effect of in-reactor exposure fast neutron (E > 1 MeV) irradiation on corrosion of Zircaloy rods by including the relationship:

$$W_{RAD} = R\, \phi_f\, t \quad (2.95)$$

where W_{RAD} is the irradiation induced corrosion weight gain,

R is the proportionality constant for irradiation induced corrosion,

ϕ_f is the fast neutron flux (E > 1 MeV), and

t is the exposure time.

The total weight gain is obtained by adding the thermal weight gain and the irradiation induced weight gain.

$$W_{TOT} = W_{TH} + W_{RAD} \quad (2.96)$$

The Chort model calculates the post-transition corrosion rate by repeated iteration of the cubic pre-transition formula to produce a cyclic oxide growth behavior. In order to compare Chort calculations with commercial power reactor experience, a temperature-dependent irradiation

induced corrosion enhancement factor (F_T), was experimentally determined for commercial power reactors. It is found to be:

$$F_T = 2.343 \text{ X } 10^3 \exp [-0.011557 \text{ x } T] \quad (2.97)$$

where F_T is the in-reactor enhancement factor, and

T is the cladding surface temperature in °K.

With this model, the total corrosion weight is obtained by multiplying the thermal weight gain calculated from equation (2.94) by the enhancement factor.

$$W_{TOT} = F_T \text{ x } W_{TH} \quad (2.98)$$

2.2.3.2 Hillner Model

Hillner[21] extended the ex-reactor model to include the in-reactor post-transition corrosion rate of Zircaloy-2 tubing by assuming that the in-reactor post-transition corrosion rate in the PWR is a proportional to the ex-reactor post-transition corrosion rate by a factor called the acceleration factor, thus

$$R' = A \text{ x } R \quad (2.99)$$

where R' is the in-reactor post-transition rate of Zircaloy,

R is the comparable ex-reactor rate, that is equation (2.84) in Hillner ex-reactor model, and

A is an empirical constant, labeled as an enhancement or acceleration factor.

The enhancement factor can be written as a function of the neutron fast flux as:

$$A = B\ (\phi)^{b} \qquad (2.100)$$

where ϕ is the post-transition fast neutron flux ($n/cm^2 \cdot s$),

B and b are experimentally determined, temperature independent constants.

The general expressions for the in-reactor post-transition corrosion rate of α-annealed and cold worked Zircaloy-2 tubing is given by:

$$R' = 8.098 \times 10^{-5}\ \phi\ \exp\ [-12529/T] \qquad (2.101)$$

For α-annealed Zircaloy-2 the minimum fast neutron flux to consider its effect or corrosion rate is:

$$\phi_{min}(\alpha) = 1.38 \times 10^{12}\ n/cm^2 \cdot sec \qquad (2.102)$$

for ß-quenched material

$$R'_{\beta} = 6.478 \times 10^{-5}\ \phi\ \exp\ [-12529/T] \qquad (2.103)$$

and the minimum fast neutron flux for ß-quenched Zircaloy

$$\phi_{min}\ (\beta) = 1.73 \times 10^{12}\ n/cm^2 \cdot sec \qquad (2.104)$$

for $\phi \leq \phi_{min}$ only the ex-reactor equations should be employed.

2.2.3.3 McDonald Model

The long-term effects of lithium hydroxide on the corrosion behavior of Zircaloy-4 in PWR's were investigated by McDonald, et al.[23]. The corrosion data were generated at 589 K, 616 K, and 633 K and summarized in Figure (2.8), which show the weight gain data as a function of total exposure time, however the lithium concentration is higher than what have been used for normal operating condition of PWR's

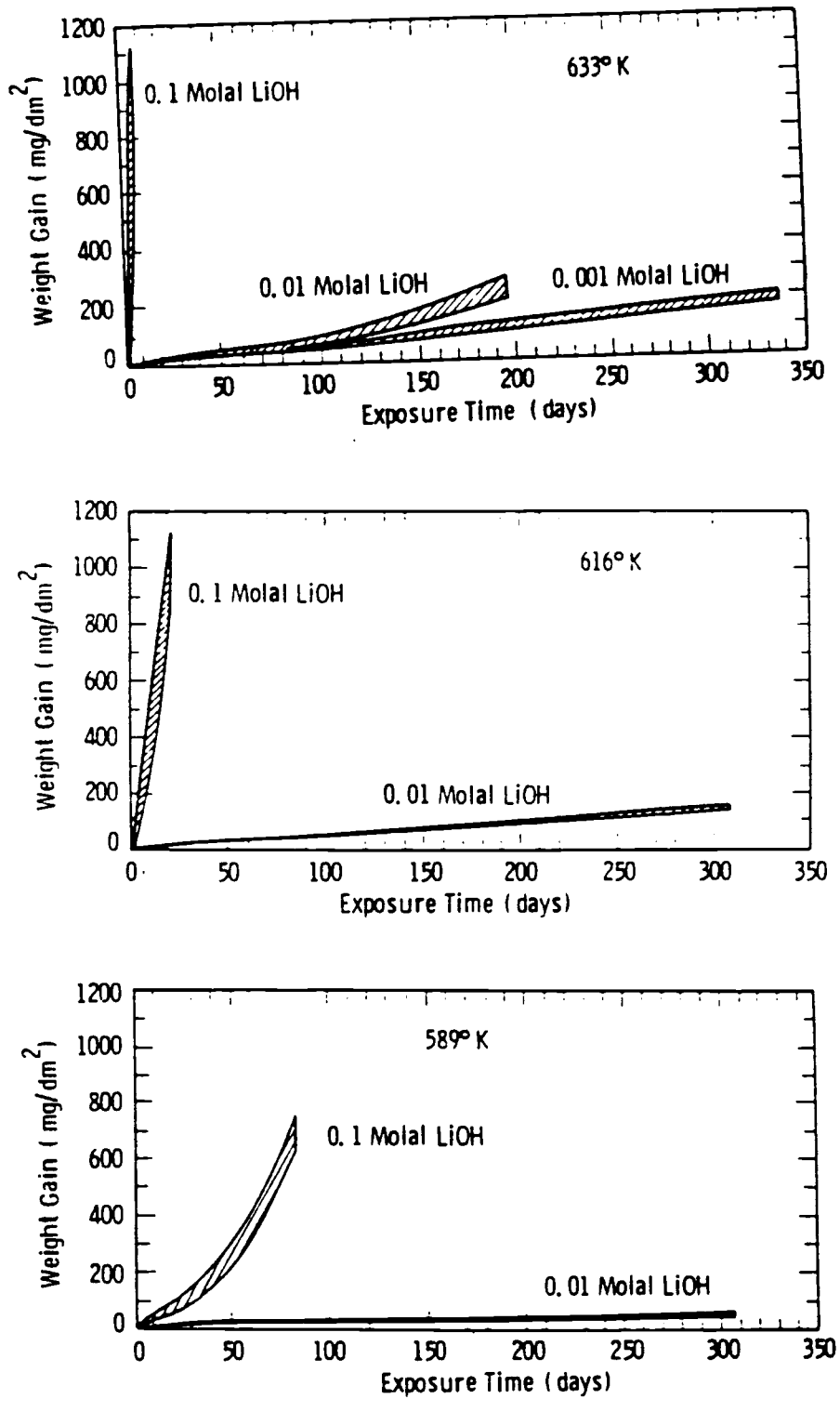

Figure 2.8 Lithium hydroxide corrosion data obtained at 589 K, 616 K, and 633 K[23].

coolant which typically range from $3x10^{-5}$ to $3x10^{-4}$ molal. The post-transition corrosion rate equation is given by:

$$\ln\left(\frac{\partial w}{\partial t}\right) = 25.39 + 185.6[Li] - 407.4[Li]^2 - \frac{(32660 + 110540[Li])}{RT} \quad (2.105)$$

where $\frac{\partial w}{\partial t}$: post-transition rate, $mg/dm^2/day$,

[Li] : Lithium hydroxide concentration, moles/liter,

R : gas constant, 1.987 cal/K-mole, and,

T : corrosion temperature, °K.

This investigation shows that, a lithium hydroxide concentration equal to or greater than 0.1 molal can lead to significant accelerated corrosion, particularly at higher oxide-metal interface temperature, and the pre-transition region disappears for higher concentration because of the corrosion acceleration.

2.2.3.4. Pyecha Model

The model developed by Pyecha[22] was generated from measurements of the oxide formed on the waterside surface of 132 reactor-irradiated rods with various fuel burnups. The development of this model is based on the temperature time dependent ex-reactor oxidation behavior and extended to include the in-reactor effects of heat flux and fast neutron flux. The following equations represent the corrosion rate for the pre-and post-transition period.

In the pre-transition region the oxide thickness change with time is found to be:

$$\frac{\partial s}{\partial t} = \frac{A}{S^2} \exp\left[-\frac{Q_1}{RT}\right] \tag{2.106}$$

Post-transition oxide thickness change with time is given by:

$$\frac{\partial s}{\partial t} = C \exp\left[-\frac{Q_2}{RT}\right] \tag{2.107}$$

and $$C = C_o + U\ (M\phi)^P \tag{2.108}$$

oxide thickness at transition:

$$S_t = D \exp\left[-\frac{Q_3}{RT}\right] \tag{2.109}$$

where $\frac{\partial s}{\partial t}$ is the oxidation rate, μm/d,

S is the oxide thickness, μm,

T is the metal-oxide interface temperature, °K,

ϕ is the fast neutron flux, n/cm^2·sec,

R is the universal gas constant, cal/mol.°K

and the constants which were determined experimentaly are:

$A = 6.3 \times 10^9\ \mu m^3/d$

$C_o = 8.04 \times 10^7\ \mu m/d$

$D = 2.14 \times 10^7\ \mu m$

$E = 1.17 \times 10^{-2}\ 1/K$

$P = 0.24$

$M = 7.46 \times 10^{-15}\ cm^2 \cdot sec/n$

$Q_1 = 32,289$ cal/mol

$Q_2 = 27,354$ cal/mol

$Q_3 = 10,763 \quad \mu m/d$

$U = 2.59 \times 10^8 \ \mu m/d$

The predicted and measured oxide thickness are in very good agreement for groups of rods having similar power history. However, the model is very temperature sensitive and has a tendency to overpredict the oxide thickness.

2.2.3.5. Forsberg Model

The Forsberg and Massih[24] model accounts for the breakaway transition in the Zircaloy oxidation rate that take place in an isothermal condition and the change in oxidation rate that occurs during reactor operation. This model is coupled to a PWR thermal and hydraulic model to study the effect of changes in coolant inlet temperature, mass flow rate, system pressure, and power history on Zircaloy oxide growth. For the pre-transition the following correlation is considered,

$$\frac{\partial s}{\partial t} = \frac{A}{s^2} \exp\left[\frac{-Q_1}{RT}\right] \tag{2.110}$$

where $\frac{\partial s}{\partial t}$ is the corrosion rate,

s is the oxide layer thickness,

T is the metal-oxide interface temperature in K,

R is the universal gas constant and

A and Q, are constants.

The temperature change through the oxide layer formed in a given time step in the power history is given by:

$$T = T_o + f\ (S-S_o) \tag{2.111}$$

where $f = \frac{q}{\lambda_{ox}}$, q is the heat flux, $\frac{W}{m^2}$,

λ_{ox} is the oxide thermal conductivity, $\frac{W}{mK}$,

S is the current oxide thickness,

S_o is the oxide layer thickness associated with the temperature T_o in the proceeding time step.

In post-transition the oxide thickness is assumed to increase linearly with time according to:

$$\frac{\partial S}{\partial t} = C \exp\left[\frac{-Q_2}{RT}\right] \tag{2.112}$$

Where C and Q_2 are empirical constants.

To account for the neutron flux enhancement factor equation (2.112) is modified to:

$$\frac{\partial S}{\partial t} = CE \exp\left[\frac{-Q_2}{RT}\right] \tag{2.113}$$

and $$E = 1 + D\ (S-S_c) \tag{2.114}$$

where S_c is the threshold thickness to consider the irradiation effect

for $S < S_c$, $D = 0$

The variable D is the neutron flux enhancement factor and is assumed to have the following form:

$$D = 1 + U\phi \tag{2.115}$$

where ϕ is the neutron flux, and

U is a constant determined by in-reactor oxide measurements.

2.2.3.6 Billot Model

Billot, et al.[25] developed a semi-empirical corrosion model to assess the external corrosion of Zircaloy cladding in PWR's by utilizing corrosion data obtained by a number of different test facilities. This model is mainly based on a finite element, thermal/hydraulic description of the core of a reactor or a test loop. The impact of physical/-chemical parameters such as temperature; irradiation and the processor arising from occurrence of a two-phase flow was also analyzed. The model describes the hydraulic and thermal changes which simulate the in-reactor steady state and transient conditions, together with the cladding temperature in a set of coupled channels consisting of sub-channels surrounding the analyzed fuel element. The oxide growth model was developed from an analysis of the corrosion data measured from an experimental facility. The oxidation rate in the pre-transition state is represented by cubic correlation given as follows:

$$\frac{\partial (S^3)}{\partial t} = K_{pre} \exp\left[\frac{-Q_{pre}}{RT_i}\right] \qquad (2.116)$$

The oxide thickness at transition is given by:

$$S_t = A \exp\left[\frac{-Q_{pre}}{RT_i}\right] \qquad (2.117)$$

In the post-transition region, the oxide thickness is determined with a linear correlation as follow:

$$\frac{\partial S}{\partial t} = K_{post} \exp\left[\frac{-Q_{post}}{RT_i}\right] \tag{2.118}$$

The oxide-metal temperature can be written as:

$$T_i = T_w - \frac{q_s}{\lambda} \tag{2.119}$$

where S is the oxide thickness,

t is the time,

S_t is the oxide thickness at transition,

A is a constant,

T_i is the metal-oxide interface temperature,

T_w is the wall temperature,

q is the heat flux,

λ is the oxide thermal conductivity,

K_{pre} is the Arrhenius equation constant during pre-transition phase,

K_{post} is the Arrhenius equation constant during post-transition phase,

Q_{pre} is the activation energy during pre-transition phase,

Q_{post} is the activation energy during post-transition, and

R is the ideal gas constant

The oxide thickness at an axial elevation (Z) of the cladding for the post-transition phase is given by:

$$S(Z) = K_{post} \sum_{1}^{N} \exp\left[\frac{-Q_{post}}{T_i(Z)}\right] t_i \tag{2.120}$$

with N_1, N_2 numbers of time steps (t_i) at Z_1, Z_2 depending on wall temperature. Also, the activation energy can be expressed as a function of the ratio of the increase in the corrosion rates at two different axial levels:

$$\frac{\Delta S(Z_1)}{\Delta S(Z_2)} = \frac{\sum_{1}^{N_1} \exp\left[\frac{-Q_{post}}{T_i(Z_1)}\right] t_i}{\sum_{1}^{N_2} \exp\left[\frac{-Q_{post}}{T_i(Z_2)}\right] T_i} \tag{2.121}$$

The irradiation effect is represented by an acceleration factor which is independent of temperature and formed oxide film as in equation (2.122). On the other hand, the effect of fast neutron flux with an energy greater than 1 MeV is represented by a multiplicative factor as a function of temperature as in equation (2.123) or by an an additive factor as a function of oxide layer thickness as in equation (2.124).

$$\frac{\partial S}{\partial t} = K\exp\left(\frac{-Q}{RT_i}\right) + C\phi \tag{2.122}$$

$$\frac{\partial S}{\partial t} = (K + C\phi^a)\exp\left(\frac{-Q}{RT}\right) \tag{2.123}$$

$$\frac{\partial S}{\partial t} = K\exp\left(\frac{-Q}{RT_i}\right) + C\phi^a S \tag{2.124}$$

where ϕ is the fast neutron flux (E >1 MeV), and

a is a constant ($0.2 < a < 1$)

The corrosion rate as a function temperature and water chemistry conditions is described by the following equations:

$$\frac{\partial (S^3)}{\partial t} = K_{pre} + F(S x Li, pH) \exp\left[\frac{-Q_{pre} + G(S x Li, pH)}{RT_i}\right] \quad (2.125)$$

$$\frac{\partial S}{\partial t} = K_{post} + F(S x Li, pH) \exp\left[\frac{-Q_{post} + G(S x Li, pH)}{RT_i}\right] \quad (2.126)$$

where $F(sxLi,pH) = a(Li)^p(pH)^q$ (2.127)

$G(sxLi,pH) = b(Li)^p(pH)^q$ (2.128)

a, b, p, q are constants which are needed to be determined experimentally.

Chapter 3

The Proposed Zircaloy Oxidation Model

The modeling procedure will be described first by constructing a model for ex-reactor (autoclave) oxidation, then this will be extended to include the factors which strongly affect the oxidation rate in PWR environments and operating conditions. A computer code (ZOM) based on a finite difference analysis has been written in FORTRAN to carry out the oxidation simulation.

3.1 Ex-Reactor Oxidation Modeling

The ex-reactor oxidation process has been modeled by employing a numerical solution generated directly from Fick's Laws. The oxygen diffusion equation for a long circular cylinder in which the diffusion of oxygen takes place in radial direction. The oxygen concentration is then a function of radius r and time t. For cylindrical geometry,

Fick's first law is given as:

$$J=-D\frac{dC}{dr} \tag{3.1}$$

and Fick's second law is shown to be:

$$\frac{\partial C}{\partial t}=\frac{1}{r}\frac{\partial}{\partial r}(rD\frac{\partial C}{\partial r}) \tag{3.2}$$

or

$$\frac{\partial C}{\partial t} = D\frac{\partial^2 C}{\partial r^2} + \frac{D}{r}\frac{\partial C}{\partial r} \tag{3.3}$$

where J is the amount of substance flowing in a unit time through a unit surface area perpendicular to the oxygen flow direction,

$\frac{\partial C}{\partial r}$ is the concentration gradient in the direction of flow, and

D is the diffusion coefficient

3.1.1 Finite-Difference Method

A fully-implicit finite difference method is constructed directly from Fick's second law for unidirectional diffusion and cylindrical coordinates. This method is chosen because of stability considerations, since this method is less restrictive to the size of the time step, Δt, which is needed for long-term oxidation modeling.

The finite difference form of the derivatives in terms of the unknown values of the concentration for the (n+1) time step become:

$$\frac{\partial^2 C}{\partial r^2} = \frac{C_{i+1}^{n+1} - 2C_i^{n+1} + C_{i-1}^{n+1}}{(\Delta r)^2} \tag{3.4}$$

$$\frac{\partial C}{\partial r} = \frac{C_{i+1}^{n+1} - C_{i-1}^{n+1}}{2\Delta r} \tag{3.5}$$

$$\frac{\partial C}{\partial t} = \frac{C_i^{n+1} - C_i^n}{\Delta t} \tag{3.6}$$

where Δt is the time increment,

Δr is the distance increment, and

i is the number of the node

The finite difference form of equation (3.3) is shown to be:

$$\frac{C_i^{n+1} - C_i^n}{\Delta t} = D\frac{C_{i+1}^{n+1} - 2C_i^{n+1} + C_{i-1}^{n+1}}{(\Delta r)^2} + \frac{D}{r}\frac{C_{i+1}^{n+1} - C_{i-1}^{n+1}}{2\Delta r} \tag{3.8}$$

$$C_i^{n+1} - C_i^n = \frac{D\Delta t}{(\Delta r)^2}\left[C_{i+1}^{n+1} - 2C_i^{n+1} + C_{i-1}^{n+1}\right] + \frac{D\Delta t}{2r\Delta r}\left[C_{i+1}^{n+1} - C_{i-1}^{n+1}\right] \tag{3.9}$$

$$-C_{i-1}^{n+1}\left[\frac{D\Delta t}{(\Delta r)^2} - \frac{D\Delta t}{2r\Delta r}\right] + C_i^{n+1}\left[1 + \frac{2D\Delta t}{(\Delta r)^2}\right] - C_{i+1}^{n+1}\left[\frac{D\Delta t}{(\Delta r)^2} + \frac{D\Delta t}{2r\Delta r}\right] = C_i^n \tag{3.10}$$

equation (3.10) can be rewritten as:

$$-R_1 C_{i-1}^{n+1} + (1 + 2R_2) C_i^{n+1} - R_3 C_{i+1}^{n+1} = C_i^n \tag{3.11}$$

where

$$R_1 = \left[\frac{D\Delta t}{(\Delta r)^2} - \frac{D\Delta t}{2r\Delta r}\right] \tag{3.12}$$

$$R_2 = \frac{D\Delta t}{(\Delta r)^2} \tag{3.13}$$

and

$$R_3 = \left[\frac{D\Delta t}{(\Delta r)^2} + \frac{D\Delta t}{2r\Delta r}\right] \tag{3.14}$$

Equation (3.11) is used to form a set of equations having a tridiagonal coefficient matrix.

$$\begin{bmatrix} (1+2R_2) & -R_3 & & & & & & \\ -R_1 & (1+2R_2) & -R_3 & & & & & \\ & -R_1 & (1+2R_2) & -R_3 & & & & \\ & & \ddots & \ddots & & & & \\ & & & \ddots & \ddots & & & \\ & & & & \ddots & \ddots & & \\ & & & & & -R_1 & (1+2R_2) & -R_3 \\ & & & & & & -R_1 & (1+2R_2) \end{bmatrix} \begin{bmatrix} C_2 \\ C_3 \\ C_4 \\ \cdot \\ \cdot \\ \cdot \\ C_{i-3} \\ C_{i-2} \\ C_{i-1} \end{bmatrix}^{n+1} - \begin{bmatrix} C_2+R_1C_I \\ C_3 \\ C_4 \\ \cdot \\ \cdot \\ \cdot \\ C_{i-3} \\ C_{i-2} \\ C_{i-1}+R_1C_{II} \end{bmatrix}^{n} \tag{3.15}$$

The stability of the fully-implicit solution for all sizes of time steps, Δt, is satisfied by using the von Neumann method [26]. A proof is given to show that this method is stable for all values of

R_1, R_2 and R_3.

To determine the stability criteria, the following equations are given:

$$\xi = \left(1 + 4R\sin^2 \frac{\beta \Delta r}{2}\right)^{-1} \tag{3.16}$$

and

$$\beta = \frac{\pi}{i\Delta r} \tag{3.17}$$

where ξ is called the amplification factor,

β is the wave number, and

R is R_1, R_2 and R_3.

The fully-implicit method is stable if $|\xi| \leq 1$, and this condition is valid for all positive values of R in equation

(3.16). Thus the fully-implicit method is stable and it has no restriction on Δt, and the long-term simulation can be attempted.

3.1.2 The Interface Equilibrium Concentration

At time zero, the oxygen concentration in the oxide is assumed to be the initial concentration as shown in Figure (3.1). For all times greater than zero, the oxygen concentration at the interfaces is assumed to be equal to the equilibrium saturation oxygen concentration. It is convenient to input this quantity as an analytical expression representing the boundary condition concentration as a function of temperature. Table (3.1) shows values of the oxygen concentration in weight percent taken from Figure (3.2) which represents the Zr-O phase diagram. These values are then converted to an oxygen concentration in g/cm^3 and presented in Table (3.2)

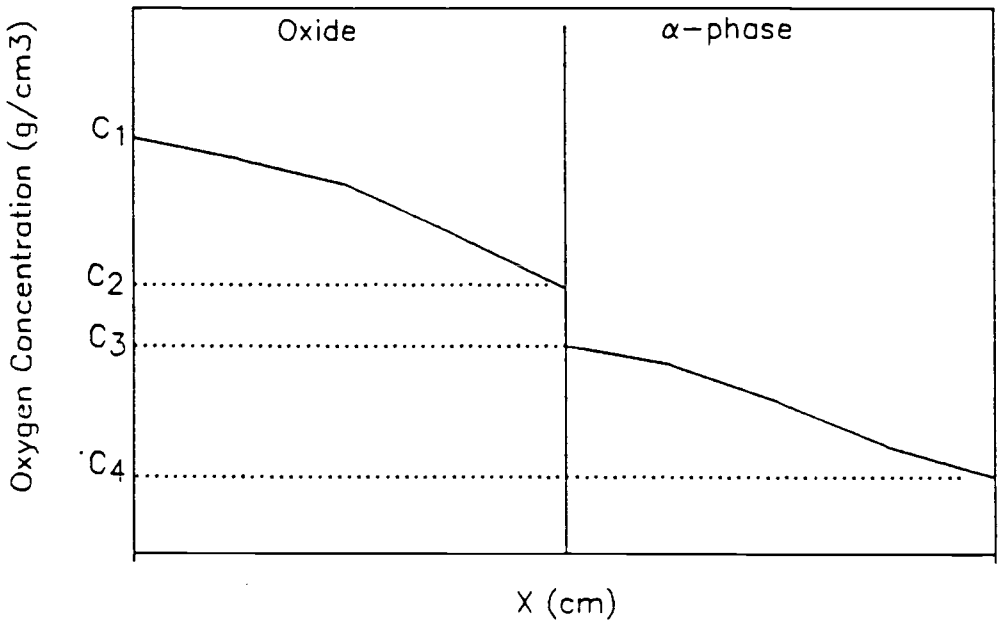

Figure 3.1 Schematic representation of the interfaces equilibrium concentration of oxygen for ZrO_2.
C_1: Coolant-oxide interface concentration at equilibrium (g/cm^3),
C_2: Oxide α-phase interface concentration at equilibrium (g/cm^3),
C_3: α-phase oxide interface concentration at equilibrium (g/cm^3), and
C_4: initial oxygen concentration in the zircaloy (9.3×10^{-4} g/cm^3)

Table (3.1) Values of the oxygen concentration in weight percent.

Concentration wt.% O	Temperature, K 2173	973
C_1	26.22	26.22
C_2	23.00	25.00
C_3	6.75	6.75

Table (3.2) Values of the oxygen concentration in (g/cm^3)

Concentration g/cm^3	Temperature, K 2173	973
C_1	1.526	1.526
C_2	1.3386	1.455
C_3	0.4387	0.4387

The equilibrium oxygen concentration C_I and C_{II} are:

$$C_I = 1.526 \ g/cm^3 \tag{3.18}$$

$$C_{II} = 1.5494 - 9.7 \times 1.0^{-5}T \quad g/cm^3 \tag{3.19}$$

where T is the absolute Temperature in K

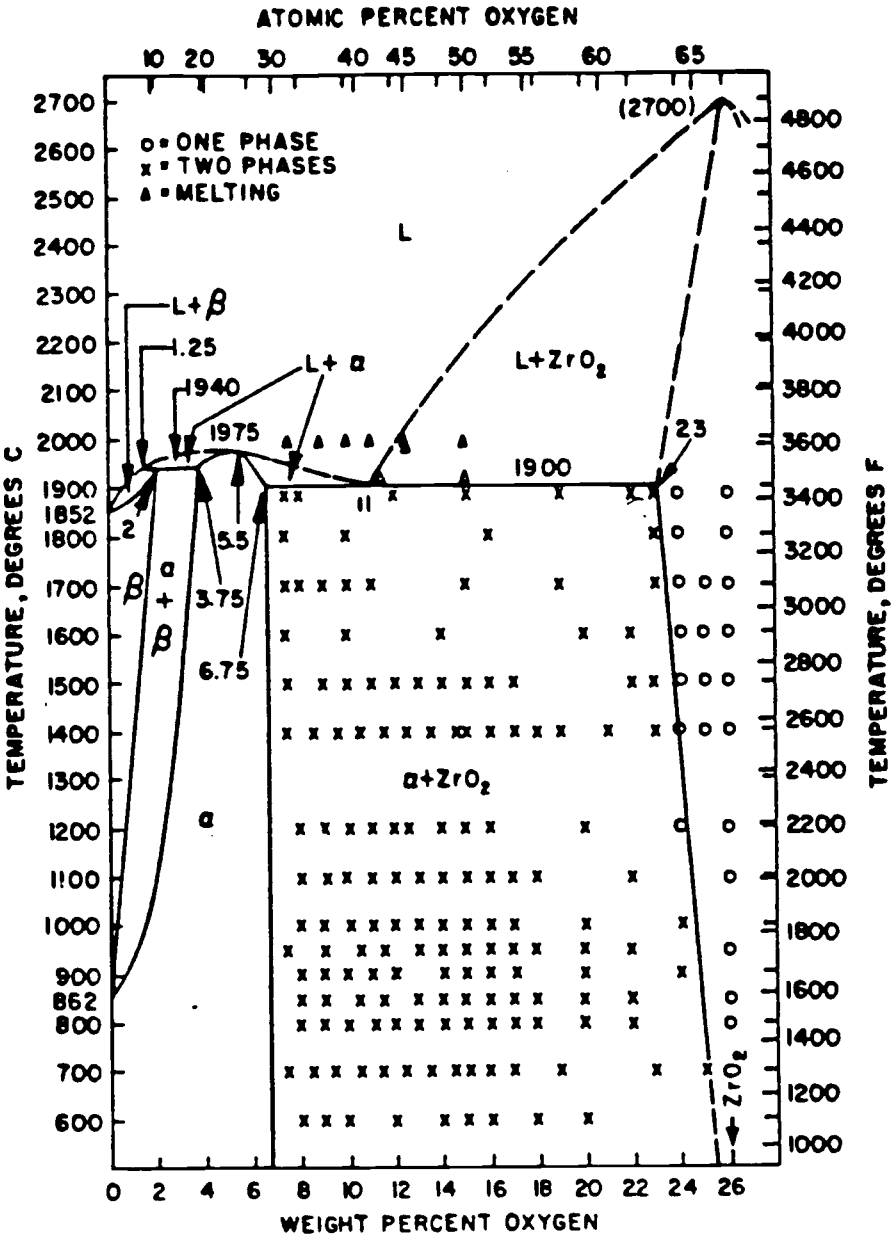

Figure 3.2 Partial diagram of Zr-O system[27].

3.1.3 Treatment of the Oxide Moving Boundary

In order to determine the motion of the oxide-metal interface during each time step, the simple version of Fick's diffusion laws is used. In this form the oxygen current is:

$$J = \frac{dm/dt}{A} = -D\frac{dC}{dr} \tag{3.20}$$

where dm: mass of matter diffusing across a distance dr in time dt, g,

D: diffusion coefficient, cm^2/sec,

A: area, cm^2, and

dC: concentration gradient across dr

Integrating this equation over the time period from 0 to t gives:

$$\int_o^m dm = \int_o^t -DA\frac{dC}{dr}dt \tag{3.21}$$

$$m = DAt\frac{dC}{dr} \tag{3.22}$$

Then, the mass of oxygen diffusing through in the oxide can be calculated as follows:

$$m = rA\rho\frac{n \cdot M}{Mw} \tag{3.23}$$

where r : oxide thickness, cm,

ρ : oxide density, g/cm^3,

n : number of atoms of oxygen in a molecule of oxide,

M : atomic weight of oxygen, and

Mw : molecular weight of the oxide.

The combination of equation (3.22) and equation (3.23) yield:

$$rA\frac{n\cdot M}{Mw}\rho = tDA\frac{\partial C}{\partial r} \tag{3.24}$$

Integrating this equation gives:

$$\int r dr = \int \frac{tDA}{\rho n\cdot MA} dC \tag{3.25}$$

and,

$$\frac{r^2}{2} = \frac{tDAMw}{\rho n\cdot MA}\Delta C \tag{3.26}$$

which therefore yields an expression for the oxide thickness as a function of time given by:

$$r = \sqrt{\frac{2DMwt\Delta C}{\rho n\cdot M}} \tag{3.27}$$

Equation (3.27) will be used to control the movement of the oxide-metal interface in the oxygen diffusion calculations.

3.1.4 Oxygen Diffusion Coefficient

The diffusion coefficient is a function of many variables such as temperature, concentration gradient and crystal structure. Typically, the diffusion coefficient is measured experimentally and expressed in the following Arrhenius form:

$$D = D_0 \exp\left(\frac{-E}{RT}\right) \tag{3.28}$$

where D_o is a constant, cm^2/sec,

E is the activation energy in Cal/mole,

R is the gas constant, cal/K-mole, and

T is the absolute temperature in °K.

Cox[28] presents a variety of diffusion coefficients for oxygen in zirconia, however these diffusion coefficients exhibit a wide variation due to the differing experimental conditions used, however a general trend is observed in that the variation is reduced at high temperature. To evaluate the long-term diffusion of oxygen in the zirconia, a new diffusion coefficient has been generated from data in the Hillner model by converting the oxide weight gain to thickness and substituting the result into equation (3.27) which can be solved for D.

$$D = \frac{x^2 \rho n \cdot M}{2 t Mw \Delta C} \tag{3.29}$$

To convert the oxide weight gain (mg/dm^2) to oxide thickness (μm) the following equation is used:

$$x = P \frac{A_z}{A_o} \times \frac{W}{\rho} \tag{3.30}$$

where x is the oxide layer thickness, μm,

P is the Pilling-Bedworth ratio (volume of oxide formed per unit volume of metal, for Zr, P = 1.56),

A_z is the atomic weight of zirconium, (91.22),

A_o is the atomic weight of oxygen, (32.0),

W is the oxide weight, mg/dm^2, and

ρ is the Zircoloy-4 density, 6.5 g/cm^3,

Therefore, inserting the above values yields:

$$x\ (\mu m) = 6.7893 \times 10^{-2}\ W\ (mg/dm^2) \tag{3.31}$$

The oxide thickness from the Hillner model[1] for both the pre-and post transition are found to be:

For pre-transition

$$x_{pre} = A\ [6.36 \times 10^{11} \exp\ (-13636/T) \times t]^{1/3}\ \mu m \qquad (3.32)$$

For post-transition

$$x_{post} = A\ [1.12 \times 10^{8} \exp\ (-12529/T) \times t]\ \mu m \qquad (3.33)$$

where $A = 6.7983 \times 10^{-2}$

Substituting the values of X in equation (3.29) gives the diffusion coefficient for the pre-transition region:

$$D_{pre} = \frac{2.4\times10^{5}}{\Delta C t^{1/3}}\left[\exp\left(\frac{-13636}{T}\right)\right]^{2/3} \quad cm^2/sec \qquad (3.34)$$

and for the post-transition conditions:

$$D_{post} = 4.0722\times10^{12}\frac{t}{\Delta C}\exp\left(\frac{-12529}{T}\right) \quad cm^2/sec \qquad (3.35)$$

The pre- and post-transition diffusion coefficients are easily related to the general empirical equation:

$$D = D_o \exp\ (-E/RT) \qquad cm^2/sec \qquad (3.36)$$

3.2 In-Reactor Oxidation Modeling

The in-reactor oxidation model is an extension of the ex-reactor model which has been described in the previous section. The in-reactor model simulates the oxidation of Zircaloy in PWR environments and conditions with number of factors used to accelerate the oxidation rate. Factors such as the heat flux and its associated thermal gradient, the influence of fast neutron irradiation, and the lithium concentration in the primary coolant water are considered.

3.2.1 Influence of the Heat Flux on the Corrosion Rate

In PWR's, the heat flux through the oxide affects the thermal gradient and specifically the temperature of the oxide-metal interface. The increase in the heat flux increases the interface temperature. With continued build up of the oxide layer, which has a low thermal conductivity compared to the Zircaloy, there will be an increased resistance to the heat transfer. Thus the interface temperature will be raised and accordingly the corrosion rate. For a cylindrical geometry represented by Figure (3.3), the amount of heat leaving the fuel element can be mathematically described by:

$$q_s = k_c A^c_{lm} \frac{(T_c - T_i)}{s} \qquad \text{(Cladding)} \qquad (3.37)$$

$$= k_x A^x_{lm} \frac{(T_i - T_s)}{x} \qquad \text{(Oxide)} \qquad (3.38)$$

where q_s : heat transfer rate, W,

k_c : clad thermal conductivity (W/m·K),

k_x : oxide thermal conductivity (W/m·K),

A^c_{lm}: clad log-mean area (m^2),

A^x_{lm}: oxide log-mean area (m^2),

x : oxide thickness (m),

s : clad thickness (m),

T_c : fuel-clad interface temperature (K),

T_i : clad-oxide interface temperature (K), and

T_s : wall temperature (K)

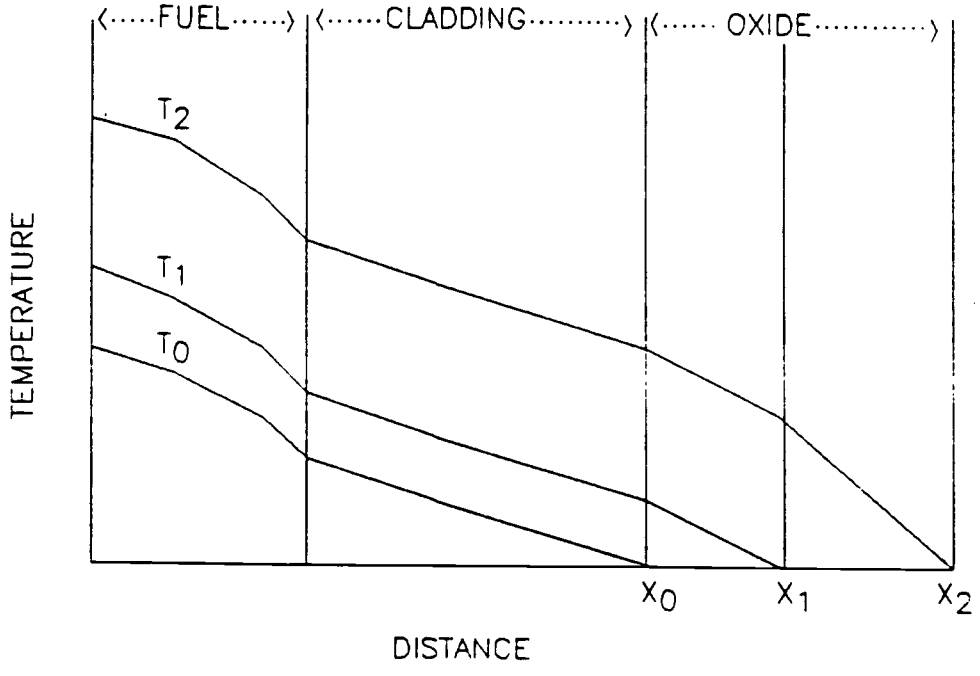

Figure 3.3 Schematic representation of the temperature profile across the fuel element

The thermal conductivity of the Zircaloy-4 as a function of temperature is given by[29]:

$$k_c = 7.848 + 2.2\times10^{-2}T - 1.676\times10^{-5}T^2 + 8.712\times10^{-9}T^3 \quad (W/m\cdot K) \tag{3.39}$$

The thermal conductivity of the oxide as a function of temperature is given by[29]:

$$k_x = 1.9599 - 2.41\times10^{-4}T + 6.43\times10^{-7}T^2 - 1.94\times10^{-10}T^3 \quad (W/m\cdot K) \tag{3.40}$$

Both the clad and the oxide thicknesses are function of time, so the new value of the clad thickness at each oxide increment can be calculated by using the following equation:

$$S' = S - \frac{x}{P} \tag{3.41}$$

where S is the clad thickness at time zero,

S' is the clad thickness at time greater than zero,

x is the oxide thickness, and

P is the Pilling-Bedworth ratio.

The log-mean area:

$$A_{lm}^{c} = \frac{2\pi xL}{\ln\left[\frac{R+S'+x}{R+S'}\right]} \tag{3.42}$$

$$A_{lm}^{x} = \frac{2\pi SL}{\ln\left[\frac{R+S'}{R}\right]} \qquad (3.43)$$

3.2.2 Effect of Irradiation

Irradiation appears to enhance the corrosion rates, especially at low temperatures, where the ex-reactor corrosion rates are very low. The most effective part is played by the fast neutrons which modify the structure of the oxide and cause radiolysis of the coolant. To account for the fast neutron flux effect, Pyecha[22] developed an empirical relation which can be used to relate the in-reactor corrosion rate to the ex-reactor rate for times after transition. The ratio between the oxidation rate with and without irradiation is given by:

$$\frac{x'}{x} = \frac{C_o + U(M\phi)^P}{C_o} \qquad (3.44)$$

where x' : the in-reactor post-transition oxide thickness,

x : the comparable ex-reactor oxide thickness,

ϕ : the fast neutron flux, n/cm^2 sec,

$C_o = 8.04 \times 10^7$ μm/d

$U = 2.59 \times 10^8$ μm/d

$M = 7.46 \times 10^{-15}$ cm^2·sec/n

$P = 0.24$

Inserting these values into equation (3.44) gives:

$$\frac{x'}{x} = \frac{8.04\times10^{7}+2.59\times10^{8}[7.46\times10^{-15}\phi]^{0.24}}{8.04\times10^{7}} \qquad (3.45)$$

Therefore,

$$\frac{x'}{x} = 1+3.2214[7.46\times10^{-15}\phi]^{0.24} \qquad (3.46)$$

where $\frac{x'}{x}$ is the enhancement factor induced by the fast neutrons.

3.2.3 Effect of Coolant Chemistry

The slight variations in the reactor coolant chemistry induced by lithium hydroxide and other chemicals can cause some changes in the oxidation kinetics. These chemicals are employed for a variety of reasons. For example, the lithium hydroxide is used to maintain the primary water system in an alkaline condition to regulate the amount of insoluble corrosion products in the coolant. This can result in a significant reduction in the primary water radiation level by reducing the amount of radioactive metals dissolved in the coolant, and a reduction in the Zircaloy corrosion resistance due to the presence of the lithium hydroxide is also experienced. This can be attributed to the increase in the anion vacancy concentration in the oxide due to the substitutional solution of lithium in the oxygen-deficient zirconium dioixde corrosion film. Hillner and Chirogs[30] showed that the rational rate

constant for the process should be directly proportional to the anion vacancy concentration in the oxide. Thus:

$$K_r^o = BC_{av}^o \tag{3.47}$$

where K_r^0: rational rate constant for pure ZrO_2,

B : proportionality constant, and

C_{av}^0: equilibrium anion vacancy concentration in the absence of any appreciable foreign ion concentration in the corrosion product. The subscript av stands for anion vacancy.

The ratio of rate constants for the corrosion kinetics with and without lithium in the oxide becomes,

$$\frac{K_r}{K^o} = 1 + \frac{3[Li^+]_{ZrO_2}}{2C_{av}^o} \tag{3.48}$$

where K_r : rational rate constant in the presence of Li^+ in the oxide,

$[Li^+]_{ZrO_2}$: lithium concentration in ZrO_2, and

C_{av}^0: equilibrium anion vacancy cocentration ($\simeq 2 \times 10^{21}$ anion vacancies per cm^3 of zirconium dioxide)

The second term in equation (3.48) can be considered as the lithium contribution to the total vacancy concentration in the corrosion product exposed to lithiated water. The concentration of lithium in the oxide is related empirically to the concentration of the lithium in aqueous solution by:

$$[Li^+]_{ZrO_2} = D[Li^+]_{H_2O} \tag{3.49}$$

where D is the distribution coefficient, a constant which has an average value of 5.

since C_{av}^0 in equation (3.48) is in units of a quantity per

cubic centimeter of oxide, it would be advantageous to employ an expression that will produce the $[Li^+]_{ZrO_2}$ concentration directly in these units. And since, 1 ppm $[Li^+]_{ZrO_2}$ is equivalent to 5 x 10^{17} atoms Li/cm^3 ZrO_2

Equation (3.49) can be written as:

$$[Li^+]_{ZrO_2} = 5 \times 10^{17} D [Li^+]_{H_2O} \quad (3.50)$$

where D : constant, 5

$[Li^+]_{ZrO_2}$: concentration of Li^+ in the oxide, atoms/cm^3 ZrO_2

$[Li^+]_{H_2O}$: concentration of Li^+ in water, ppm

From equation (3.48) and equation (3.50) a simple equation can be obtained to determine the lithium concentration effect on the oxidation rate of the Zircaloy.

$$\frac{K_r}{K_r^o} = 1 + \frac{3\times5\times10^{17}\times5[Li^+]_{H_2O}}{2\times2\times10^{21}} \quad (3.51)$$

$$\frac{K_r}{K_r^o} = 1 + 1.875\times10^{-3}[Li^+]_{H_2O} \quad (3.52)$$

where $[Li^+]_{H_2O}$ is the concentration of Li^+ in water, ppm.

or

$$\frac{K_r}{K_r^o} = 1 + 13.125[Li^+]_{H_2O} \quad (3.53)$$

where $[Li^+]_{H_2O}$ is the concentration of Li^+ in water, moles/liter.

Chapter 4

Results and Discussion

The prediction of the long-term corrosion rate of Zircaloy-4 in water, can be achieved by solving the oxygen diffusion equation numerically and by using the proper moving boundary equation to control the motion of the oxide-metal interface. However, the available diffusion coefficients in the literature are not adequate to describe the diffusion of the oxygen ions in the oxide, thus an accurate simulation for the oxidation process cannot be produced. This short-coming can be related to some reasons as follows: (1) The published diffusion coefficients were developed for the high temperature range, not less than 673 K. This is beyond the normal operating conditions of the nuclear power reactors. (2) The values of the published diffusion coefficients show considerable scatter. (3) The diffusion coefficients are represented by Arrhenius Law, such as: $D = D_o \exp(-Q/RT)$, which is not adequate to be used to describe the diffusion for both the pre- and post-transition regions.

One aim of this study is to develop an accurate value for the diffusivity of oxygen in the oxide during the oxidation process of Zircaloy-4 in water over the temperature range 533K-673 K. The determination of the diffusion coefficients for the pre- and post-transition regions was

made possible by solving equation (3.26) for the diffusion coefficient, then substituting the oxide thickness, X, with the Hillner model results which have been converted from weight gain to oxide thickness. This new diffusion coefficient, which depends on the oxidation temperature and the oxygen gradient concentration in the oxide, makes it possible to develop a model which simulates the pre- and post-transition oxidation.

Figure (4.1) shows the diffusion coefficients generated by this method at different temperatures in the range of 550 K - 710 K. From this figure it is clear that the diffusion coefficients are a function of the oxide thickness, which can be related to the oxygen concentration gradient. At high temperatures, for example 710 K and higher, it is possible to ignore the pre-transition region, because it takes very little time to reach the transition point and most of the oxide thickness is produced during the post-transition period. The diffusion coefficients decrease during the pre-transition period in proportion to the oxygen concentration gradient. For the post-transition region it starts to increase gradually, according to the increased growth of the cracks and pores in the oxide structure, which accelerate the diffusion of oxygen ions in the oxide. The predicted values of the diffusion coefficients are compared with some experimental values, as shown in Figures (4.2) through (4.6). The experimental values

which were given by Cox[28] have been presented as constant values along the oxide thickness, since they were determined only as a function of temperature according to the Arrhenius law. Figure (4.2) shows the diffusion coefficient at 550 K, which was generated by this model compared with experimental data. There is a significant scattering between the values which were presented by Kingery, et al.[28] and the data given by Douglass[28], however this variation becomes less at higher temperatures, such as 710 K, as shown in Figure (4.6). Figures (4.3), (4.4) and (4.5) show the same behaviour, however as the temperature goes up it takes less time to reach the transition point and it induces more acceleration to the diffusion process. The predicted diffusion coefficients always lie within the range of the experimental diffusion coefficients at the pre-transition region, which were obtained for a thin oxide film about 2 μm as mentioned by Cox[28]. This would justify the determination of the spatial dependence diffusion coefficients, particularly for the pre-transition region.

This model can be used to predict the isothermal long-term oxidation rate of Zircaloy-4 in water. The oxidation curves seen in Figure (4.7) show a transition time which is a characteristic feature of Zircaloy-4 corrosion rates in water and steam. The oxidation rate in mg/dm^2 of Zircaloy-4 at low temperatures, such as 550 K, 590 K, and 630 K remain low enough to allow this alloy to be used for

long-time service in power reactors. The transition time is greatly influenced by the temperature. At low temperatures, such as 550 K for a 1,000 day oxidation time, there is no transition. But the higher the temperature, the earlier the transition point on the oxidation curve appears. During this analysis, the thermal conductivity of the oxide layer and the Zircaloy-4 are assumed to be temperature dependent, as given in Chapter 3. Similarly, Figure (4.8) shows the oxide thickness versus time and the same discussion can be repeated here.

In power reactors, the heat fluxes are high enough to influence the oxide-metal interface temperature. For this reason, the assumption that the oxide-metal interface temperature is the same as the local water temperature is no longer valid. The influence of the heat flux is considered according to the analytical approach presented in Chapter 3. For various values of the heat flux, an acceleration in the corrosion process is noticed, as seen in Figure (4.9). At temperatures of 620 K, and for oxidation time equal to 1,000 days, the oxide thickness grows rapidly with the increase of the heat flux. For isothermal conditions at 620 K, the oxide thickness reaches about 14 μm. For the same waterside temperature and heat flux of 50 W/cm^2, the oxide-metal interface temperature reaches about 625 K and the oxide thickness grows about 2.5 μm more. For a heat flux of 100 W/cm^2, the interface temperature

increases to about 631 K and the oxide thickness grows up to 20 μm. If the heat flux reaches 150 W/cm^2 the interface temperature increases to 643 K and the oxide thickness reaches 29 μm.

The long-term effects of low concentrations of the lithium hydroxide have been introduced by employing an empirical correlation which accounts for the effect of the lithium on the acceleration of the corrosion rate. Hillner and Chirigos[30] suggested that the oxidation rate depends on the concentration of the anion vacancies. If lithium is introduced into the Zircaloy oxide lattice, the anion vacancy concentration increases, subsequently increasing the oxygen ion diffusion, which in turn increases the diffusion, which in turn increases the corrosion rate. The prediction of the weight gain for different lithium concentrations is shown in Figures (4.10) and (4.11). The weight gain at 620 K and for 1,000 days, with no lithium hydroxide reaches about 180 mg/dm^2. For 0.01 moles/liter lithium hydroxide, it gains 20 mg/dm^2 more. When the lithium hydroxide concentration becomes 0.1 moles/liter the weight gain doubles. The bulk concentration of lithium in the pressurized water reactors coolant typically ranges from 3 x 10^{-5} to 3 x 10^{-4} moles/liter[23]. The effect of this low lithium concentration is represented in Figure (4.11), which shows that the lithium concentration within this range has a minimal effect on the corrosion rate.

In order to make reliable predictions of the corrosion rate in in-reactor situations it is necessary to know how much contribution to the total corrosion rate comes from each factor. However, some of the corrosion mechanisms and factors are not precisely and independently known. The mechanism of how the irradiation influences and accelerates the corrosion rate is not well established. Billot, et al.[25] related the increase in the oxidation rate to the change in microstructure (porosity) and in the physical/chemical environment inside the oxide layer, which grows during the post-transition phase. An enhancement factor presented in Chapter 3 is used to account for the fast neutron flux effect in the post transition region. Figure (4.12) shows the contribution of different values of the fast neutron flux and ranges from 1 x 10^{12} n/cm^2·sec to 5 x 10^{13} n/cm^2·sec, for neutron energies greater than 1 MeV. The weight gain at 620 K produced by a 1,000 day exposure grows very rapidly with increasing neutron flux. This figure gives an idea about the irradiation effect on the corrosion rate. This contribution is dominant since it produces double the weight gain for 1,000 days and 1 x 10^{12} n/cm^2·sec fast neutron flux. For 5 x 10^{13} n/cm^2·sec the weight gain increase reaches more than 650 mg/dm^2, compared to 180 mg/dm^2 for zero fast neutron flux.

Finally, the predicted values of the isothermal ex-reactor corrosion rate are compared with some experimental

data presented by Peters[31] as shown in Figure (4.13). Also, the in-reactor corrosion rate is compared with some experimental data presented by Pychea, et al.[22] as shown in Figure (4.14). The predictions of this model are in good agreement with the experimental data obtained for long-term ex- and in-reactor oxidation.

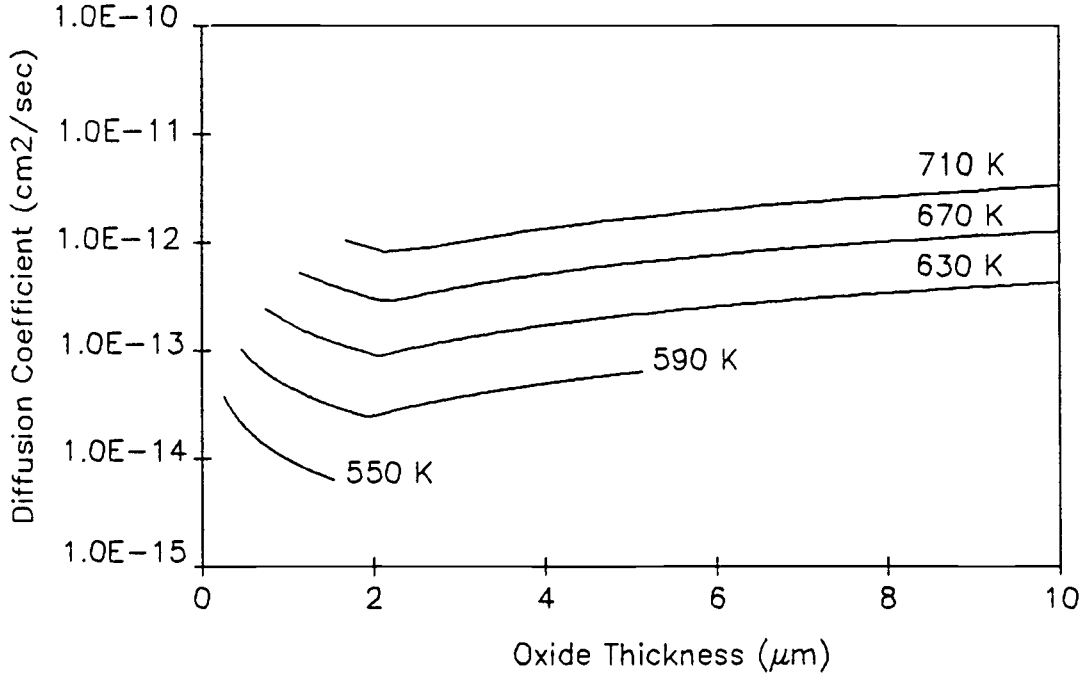

Figure 4.1 Calculated diffusion coefficients for oxygen in the oxide at different temperatures.

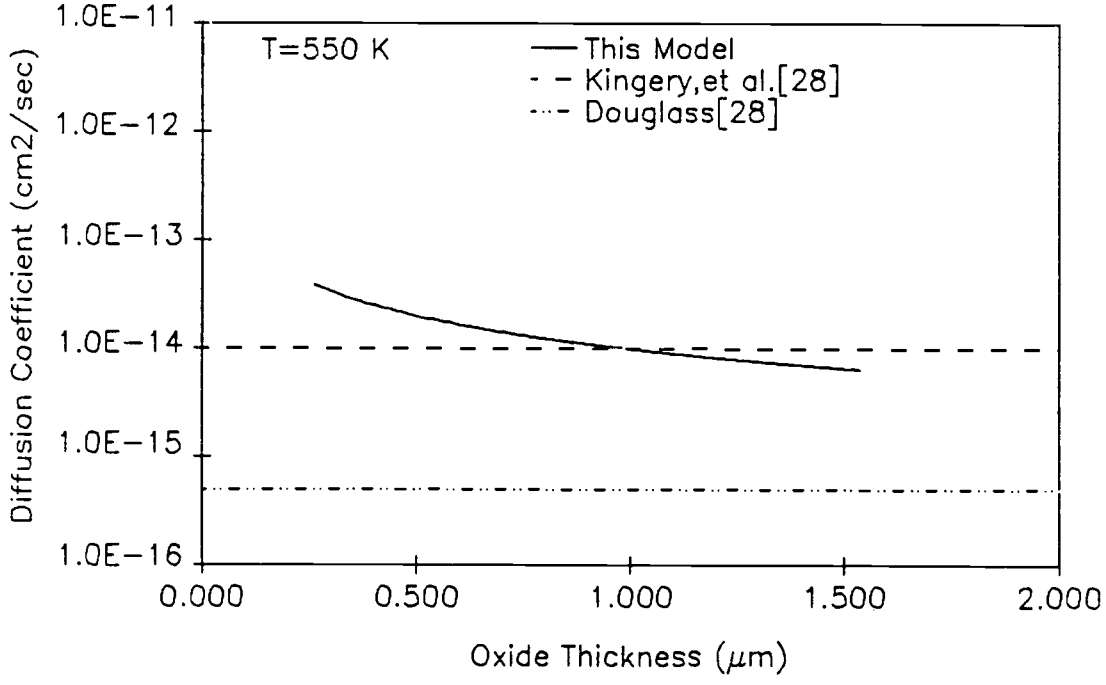

Figure 4.2 Comparison of the model prediction and measured values for the diffusion coefficient at 550 K.

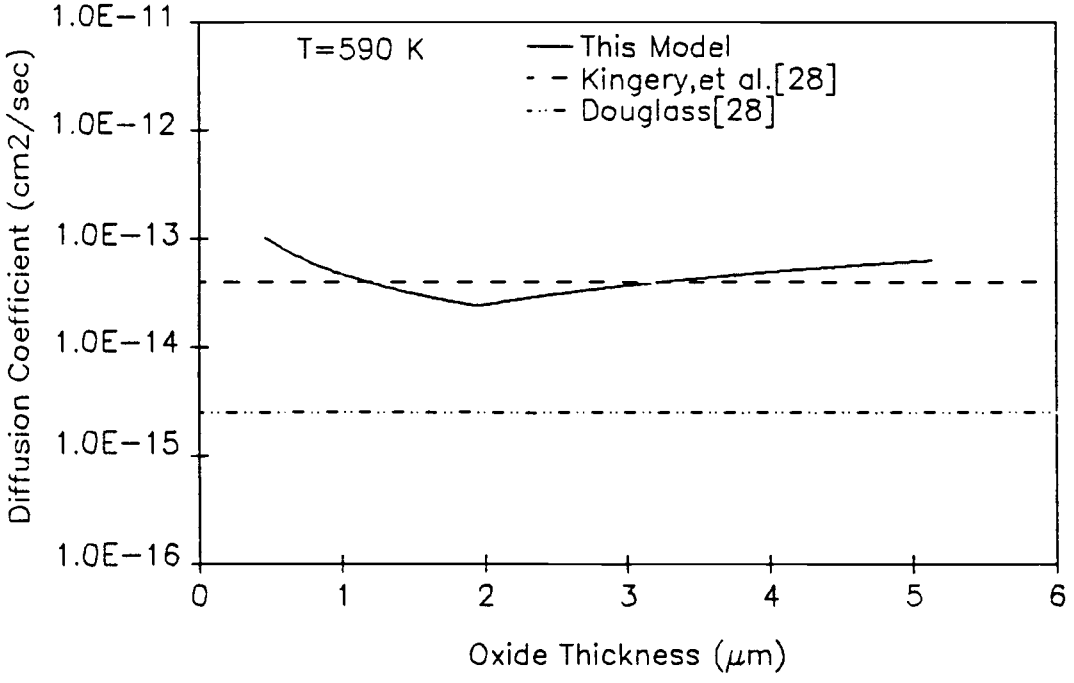

Figure 4.3 Comparison of the model prediction and measured values for the diffusion coefficient at 590 K.

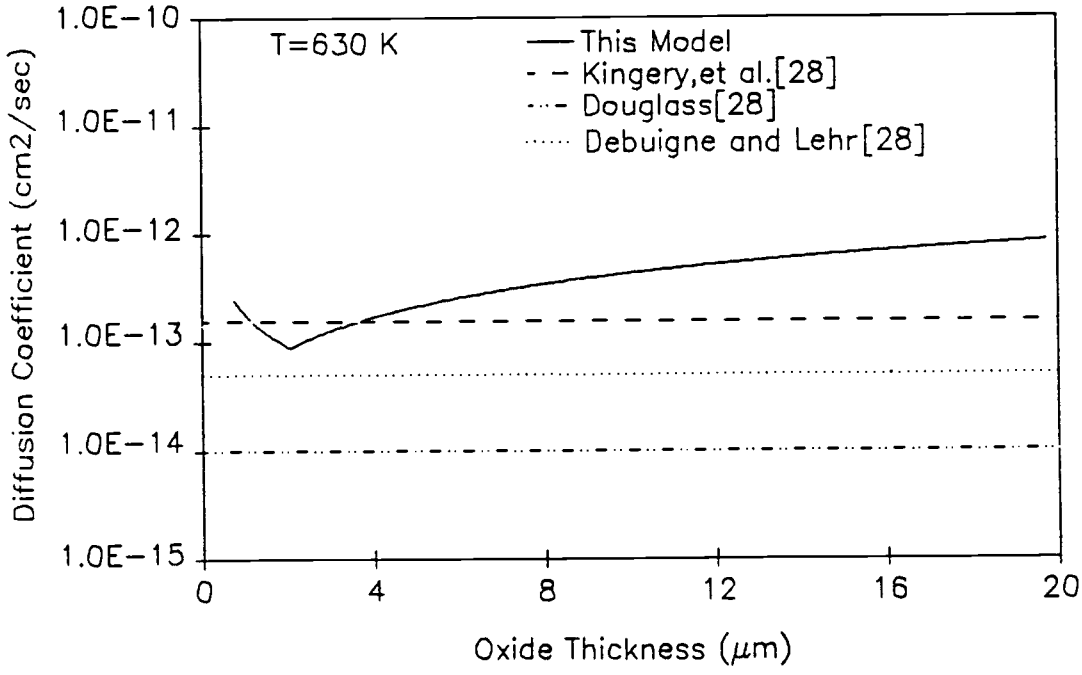

Figure 4.4 Comparison of the model prediction and measured values for the diffusion coefficient at 630 K.

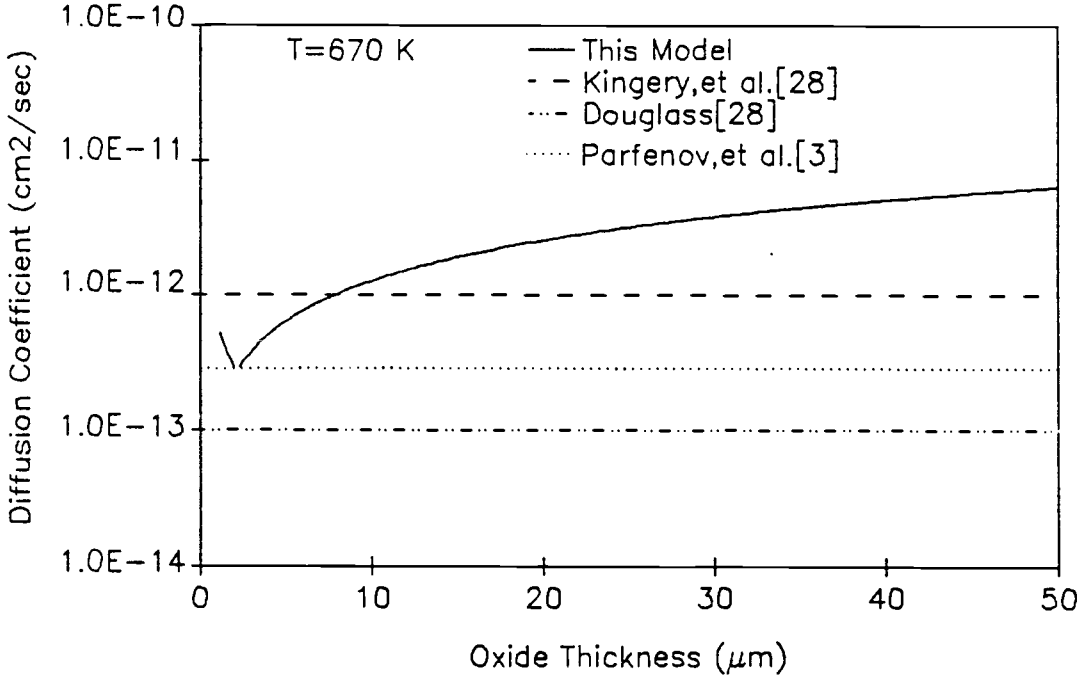

Figure 4.5 Comparison of the model prediction and measured values for the diffusion coefficient at 670 K.

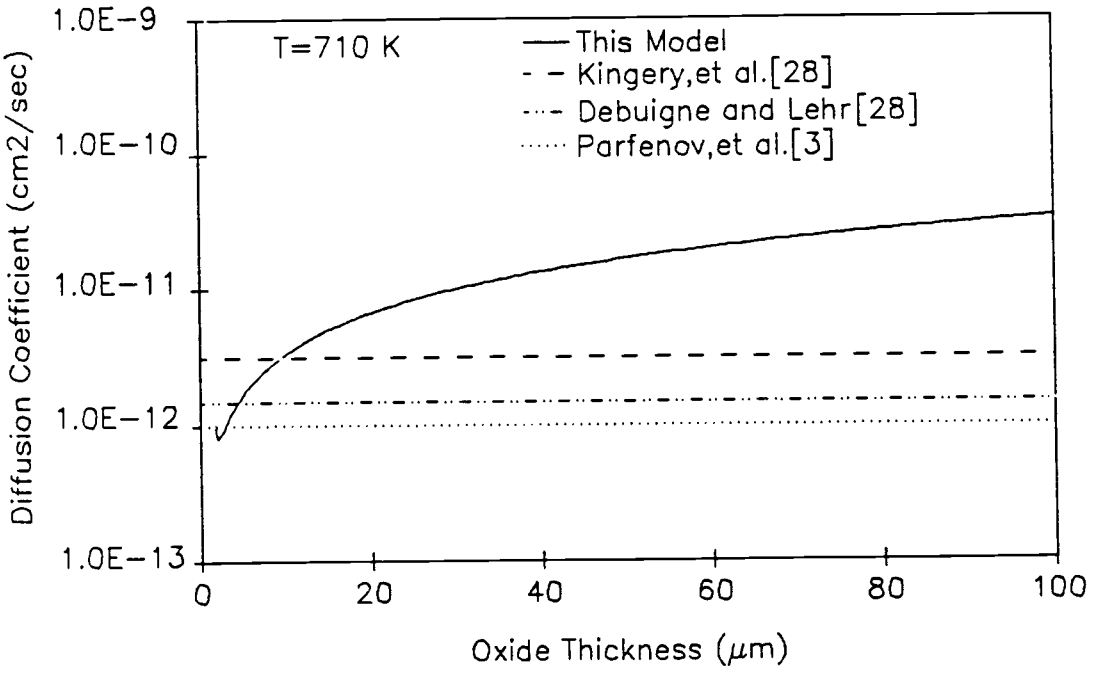

Figure 4.6 Comparison of the model prediction and measured values for the diffusion coefficient at 710 K.

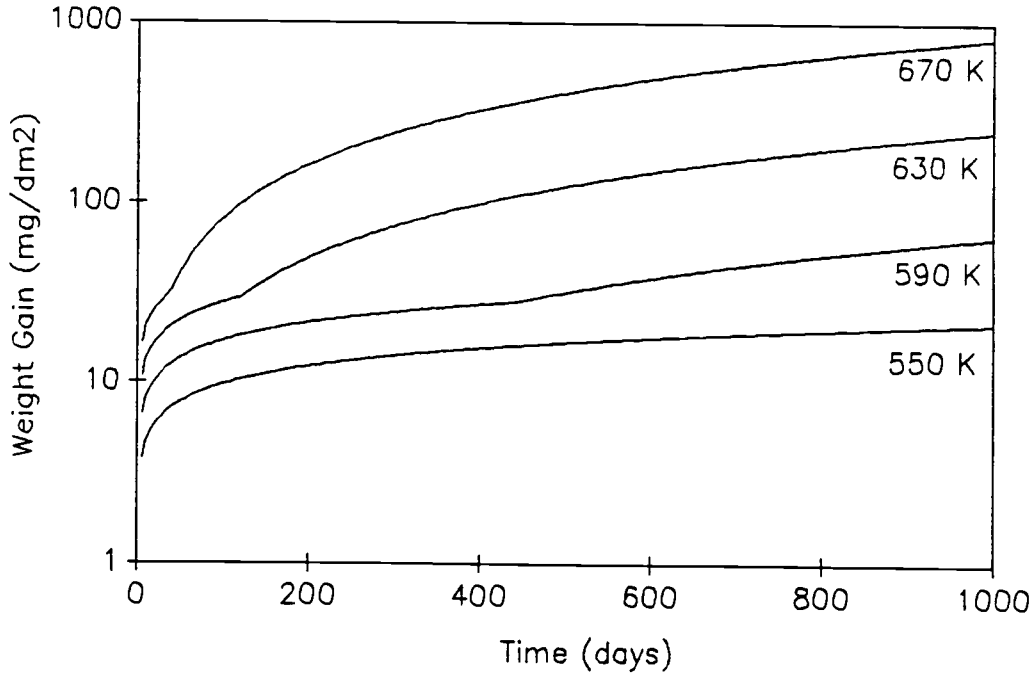

Figure 4.7 Model prediction for long-term Zircaloy-4 weight gain at different temperatures and under isothermal conditions.

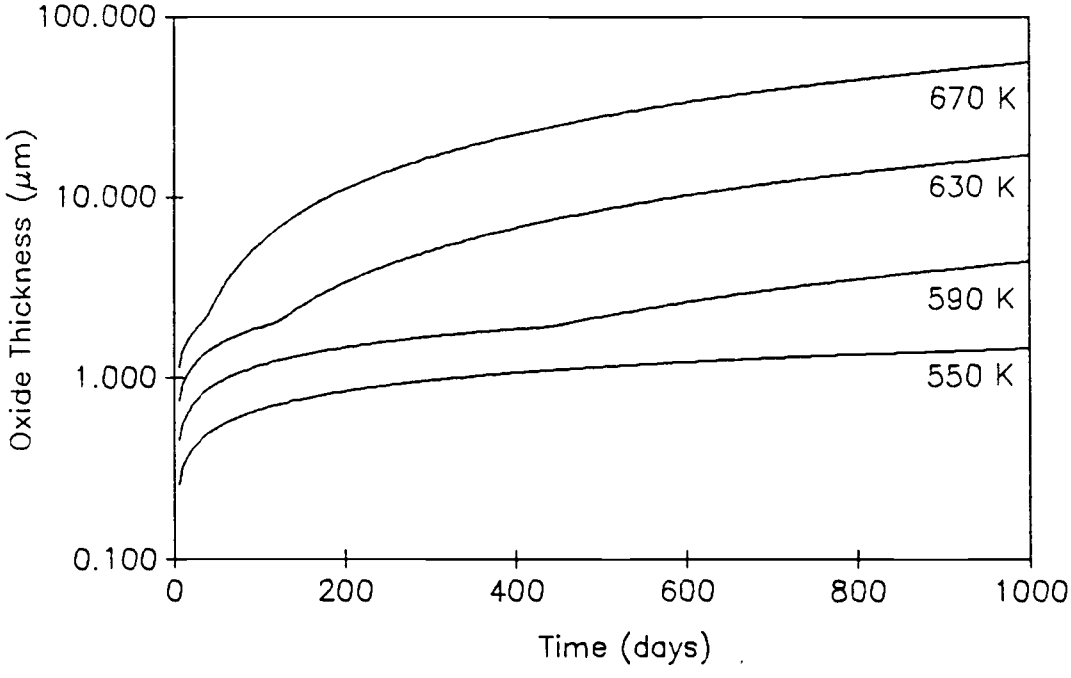

Figure 4.8 Model prediction for long-term Zircaloy-4 oxide thickness at different temperatures and under isothermal conditions.

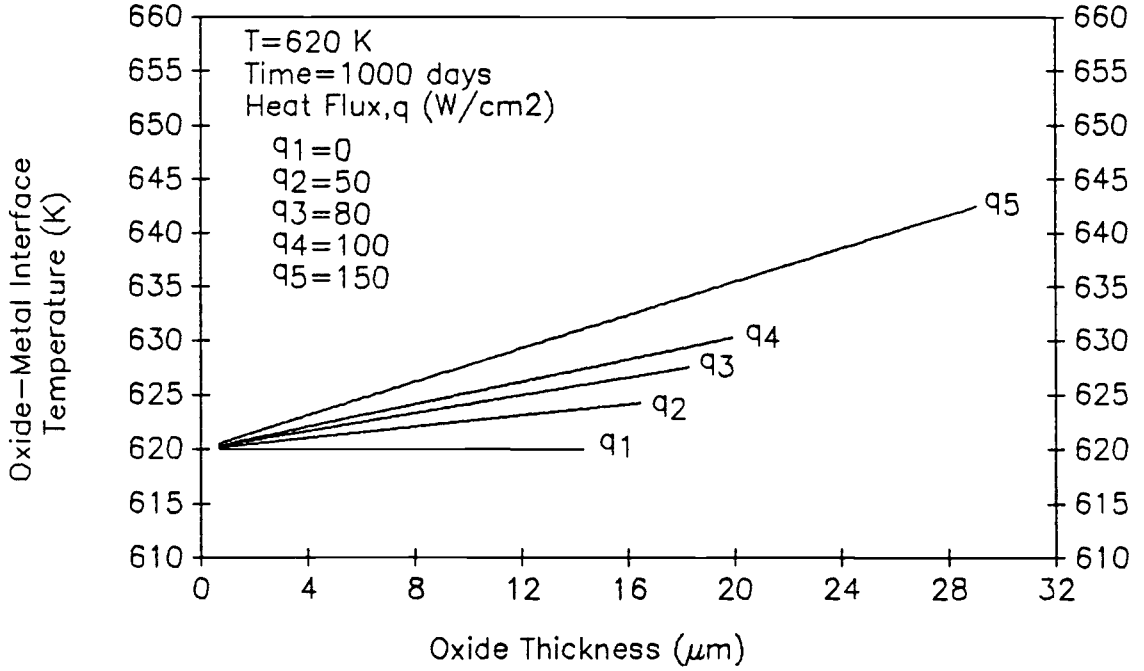

Figure 4.9 Calculated influence of heat flux on the oxide-metal interface temperature and its effect on the corrosion rate.

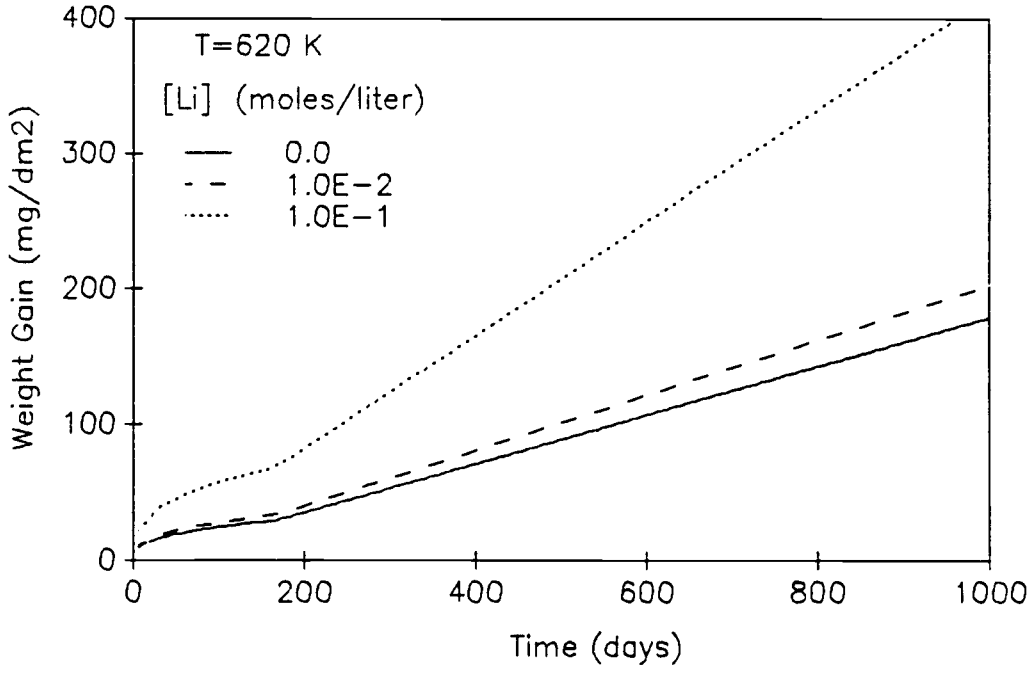

Figure 4.10 High lithium hydroxide concentration influence on the corrosion rate at 620 K.

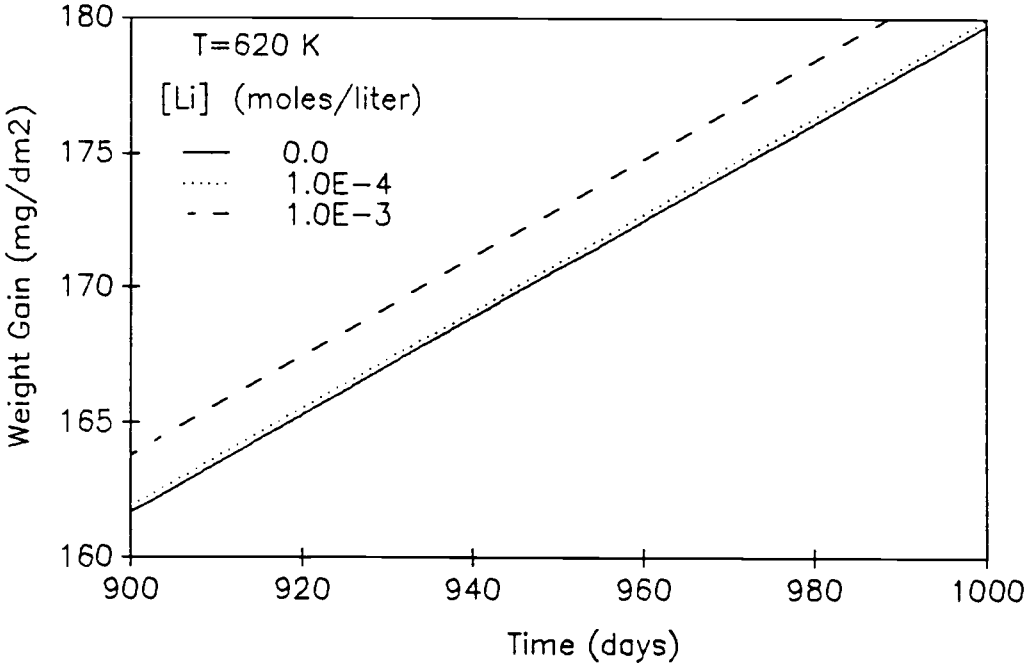

Figure 4.11 Low lithium hydroxide concentration influence on the corrosion rate at 620 K.

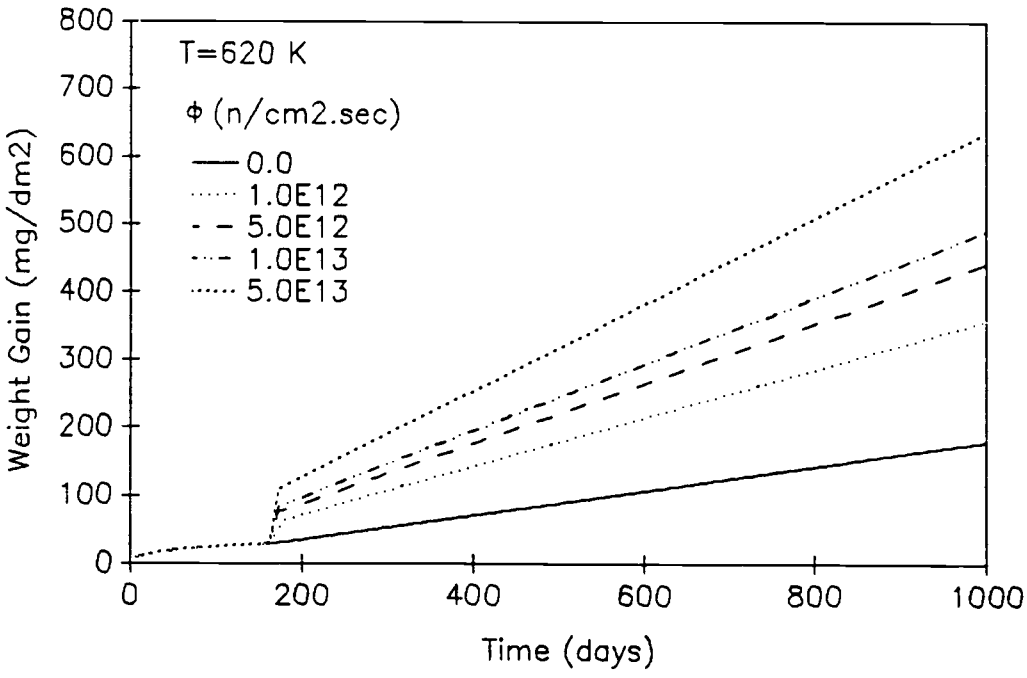

Figure 4.12 Fast neutron flux influence on the corrosion rate of Zircaloy at 620 K.

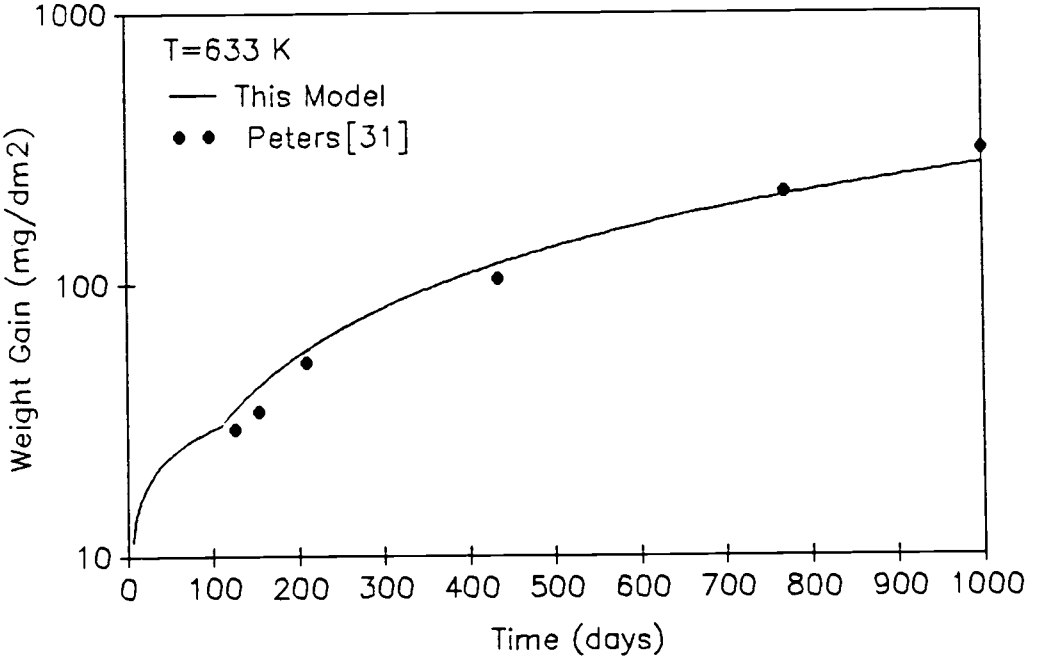

Figure 4.13 Comparison of the model prediction for long-term isothermal oxidation with measured corrosion data at 633 K.

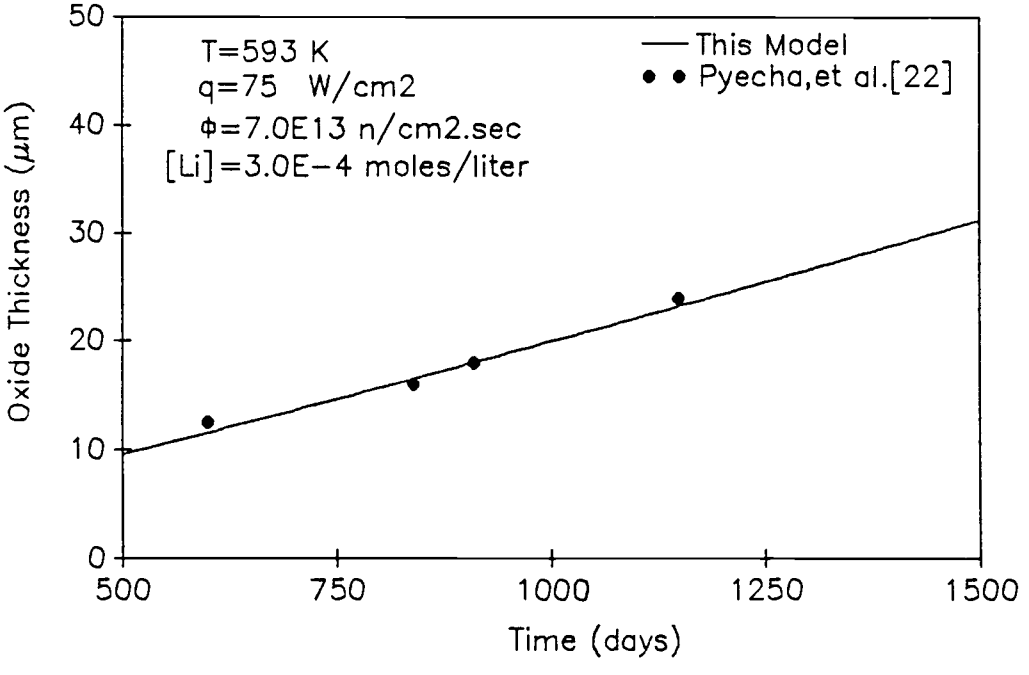

Figure 4.14 Comparison of the model prediction for long-term in-reactor corrosion rate with measured in-reactor corrosion data.

Chapter 5

Conclusions and Recommendations

A model was developed to simulate the oxidation of Zircaloy-4 and to predict the corrosion rate for ex- and in-reactors conditions in terms of weight gain and oxide thickness. The importance of this model comes from new diffusion coefficients developed to simulate the pre- and post-transition oxidation kinetics. The diffusion coefficients are shown to be functions of temperature and the oxygen concentration gradient through the oxide layer. This model permits the calculation of the Zircaloy-4 weight gain in mg/dm^2 and the oxide thickness in μm for isothermal conditions as well as in the presence of the heat flux. Also, the weight gain and the oxide thickness due to the acceleration by the lithium hydroxide and the enhancement by the fast neutron flux can be calculated. Comparison of this model predictions for isothermal ex-reactor oxidation with experimental data in the literature is presented and shows very good agreement. In conclusion, the work presented here has contributed to the understanding of the modeling of the isothermal oxidation of Zircaloy-4 and the simulation of ex-and in-reactor oxidation.

The following recommendations for further studies are proposed:

(1) The results of this model have suggested experimental efforts that can be performed to verify the validity of the developed diffusion coefficients. This can be done by the determination of the diffusion coefficient for the pre and post-transition region at different temperatures, and then to compare it with the result of this model.

(2) The Zircaloy matrix composition is believed to be a major factor in controlling corrosion rates, thus by utilizing the experimental results obtained during studies of Zircaloys oxidation can be correlated and used in this model to determine the optimum composition of alloys for PWR cladding materials.

(3) This model can be modified to study the effect of the temperature history throughout the fuel rods life time. Also, it is possible to make some modification to predict the axial oxidation rate on the fuel rod.

References

[1] Hillner, E., "Corrosion of Zirconium - Base Alloys - An Overview," Zirconium in the Nuclear Industry; Third Conference, ASTM STP 633, A.L. Lowe, Jr. and G.W. Parry, Eds, ASTM, 1977, pp. 211-235.

[2] Iglesias, F.C., Duncan, D.B., Sagat, S. and Sills, H.E. Journal of Nuclear Materials 130 (1985) 36-40.

[3] Parfenov, B.G., Gerasimov, V.V. and Vendiktova, G.I. Corrosion of Zirconium and Zirconium Alloys, translated from Russian, Jerusalem by IPST Press, 1969.

[4] Cathcart, J.V., "Zirconium Metal-Water Oxidation Kinetics," Quarterly Progress Report on the Zirconium Metal-Water Oxidation Kinetics Program sponsored by the NRC Division of Reactor Safety Research, December 1976, Oak Ridge national Laboratory, TN, Report ORNL/NUREG/TM-87, 21 January 1977.

[5] Jose, W., Diffusion in solids, Liquids, Gases (Academic Press, N.Y. 1952) p. 71.

[6] Pemsler, J.P., Journal of Nuclear Materials 7 (1962) 16-25.

[7] Rosa, C.J., Journal Less-Common Materials 15 (1968) 183-191.

[8] Pawl, R.E., Journal of Nuclear Materials 49 (1973/1974) 281-290.

[9] Dollins, C.C., and M. Jurisich, Nuclear Materials 113 (1983) 19-24.

[10] Garcia, E.A., Journal of Nuclear Materials 92 (1980) 249-256.

[11] Pemsler, J.P., Journal Electrochemical Society 111 (1964) 381-385.

[12] Wenst, R.C., CRC Handbook of Chemistry and Physics (CRC Press, Inc. Boca Raton, FL. 68th ed., 1988).

[13] Denis, A., and E.A. Garcia, Journal of Nuclear Materials 96 (1981) 127-140.

[14] Garcia, E.A., Journal of Nuclear Materials 96(1981) 118-126.

[15] Eucken, C.M, Finden, P.T., Trayp-Pritsching, S. and Weidinger, H.G., "Influence of Chemical Composition on Uniform Corrosion of Zirconium-Base Alloys in Autoclave Tests." Zirconium in Nuclear Industry: Eighth International Symposium, ASTM STP 1023, L.F.P. Van Swam and C.M. Eucken, Eds., American Society for Testing and Materials, Philadelphia, 1989, pp. 113-127.

[16] Polc, R.A., "Oxidation Kinetics and Auger Microprobe Analysis of Some oxidized Zirconium Alloys," Zirconium in the Nuclear Industry: Eighth International Symposium, ASTM STP 1023, L.F.P. Van Swam and C.M. Eucken, Eds., American Society for Testing and Materials, Philadelphia, 1989, pp. 498-514.

[17] Wadman, B. and Andren, H.-O. "Direct Measurement of Matrix Composition in Zircaloy-4 by Atom Probe Microanalysis," Zirconium in the Nuclear Industry: Eighth International Symposium, ASTM STP 1023, L.F.P. Van Swam and C.M. Eucken, Eds., American Society for Testing and Materials, Philadelphia, 1989, pp. 423-434.

[18] Carzoarolli, F., Jorde, D., Manzel, R., Parry, G.W., and Smerd, P.G., "Review of PWR Fuel Rod Waterside Corrosion Behavior." EPRI-NP-1472, Electric Power Research Institute, Palo Alto, CA, August 1980.

[19] Clayton, J.C. and Fischer, R.L., "Corrosion and Hydriding of Zircaloy Fuel Rod Cladding in 633 K Water and Reactor Environments, "In Light Water Reactor Performance, DOE/NE/34130-1, April 1985.

[20] Bryner, J.S., "The Cyclic Nature of Corrosion of Zircaloy-4 in 633 K Water," Journal of Nuclear Materials, 82, 1977, pp. 84-101.

[21] Hillner, E., "Long-Term In-Reactor Corrosion and Hydriding of Zircaloy-2 Tubing, "Zirconium in the Nuclear Industry, Fifth Conference, ASTM STP 754, D.G. Franklin, Ed., ASTM, 1982, pp. 450-470.

[22] Pychea, T.D., Bain, G.M., McInteer, W.A., and Pham, C.H., "Waterside Corrosion of PWR Fuel Rods Through Burnups of 50,000 MWD/MTU,"In Light Water Reactor Performance, DOE/NE/34130-1, April 1985.

[23] McDonal, S.G., Sabol, G.P., and Sheppard, K.D., "Effect of Lithimu Hydroxide on the Corrosion Behavior of Zircaloy-4," Zirconium in the Nuclear Industry: Sixth International Symposium, ASTM STP 824, D.G. Franklin and R.B. Adamson, Eds., American Society for Testing and Materials, 1984, pp. 519-530.

[24] Forsberg, K. and Massih, A.R., "A Model for Uniform Zircaloy Clad Corrosion in Pressurized Water Reactors, "IAEA-Technical Committee on Fundamental Aspects of Corrosion of Zirconium-Base Alloys in Water Reactors Environments, Portland, OR, September 11-15, 1989.

[25] Billot, PH. Beslu, A., Giordand, A., and Thomazet, J., "Development of Mechanistic Model to Assess the External Corrosion of Zircaloy Cladding in PWR's," Zirconium in the Nuclear Industry, Eighth International Symposium, ASTM STP 1023, 1989.

[26] Forsythe, G.E. and Wasov, W.R., Finite Differnece Methods for Partial Differential Equations, John Wiley, New Yourk, 1960.

[27] Domagala, R.F., and McPherson, D.J., Trans. AIME, 200 (1954) PP. 238-246.

[28] Cox, B. and Pemsler, J.P., Journal of Nuclear Materials 28 (1968) pp. 73-78.

[29] Ursu, I., Physics and Technology of Nuclear Materials (Pergamon Press Ltd., 1985).

[30] Hillner, E. and Chirigos, J.N., "The Effect of Lithium Hydroxide and Related Solutions on the Corrosion Rate of Zircaloy in 680° F Water," WAPD-TM-30, Westinghouse Electric Corporation, Bettis Atomic Laboratory, (August 1962).

[31] Peters, H.R., "Improved Characterization of Aqueous Corrosion Kinetics of Zircaloy-4." Zirconium in the Nuclear Industry: Sixth International Symposium, ASTM STP 824, D.G. Franklin and R.B. Adamson, Eds., American Society for Testing and Materials, 1984, pp. 507-518.

APPENDICES

Appendix A: Simulation Program (ZOM)

```
C*******************************************************************************
C*******************************************************************************
C***                                                                          ***
C***                      ZIRCALOY OXIDATION MODEL                            ***
C***                                                                          ***
C***                This program calculates the weight gain for               ***
C***                the fuel cladding materials ( Zircaloy-4 )                ***
C***                under pressurized water reactors   ( PWR )                ***
C***                operating conditions and environments as a                ***
C***                function of time in one dimensional system                ***
C***                ( cylinder ) by employing a fully implicit                ***
C***                finite difference method .                                ***
C***                                                                          ***
C*******************************************************************************
C
C                              By:
C                       Almarshad , Abdullah I.
C
C                            Instructor:
C                        Dr. Andrew C. Klein
C
C                             1.1.1990
C
C*******************************************************************************
C
C  MAIN PROGRAM
C  ------------
C   The output will be in " ZOM.OUT "
C-------------------------------------------------------------------------------
C
C  Description of input parameters:
C
C                IL     : number of grid points.
C                DX     : grid size ,cm.
C                TL     : cladding thicknes ,cm.
C                Z      : oxide thickness ,cm
C                ZU     : oxide thickness ,um
C                DT     : time step ,sec.
C                DIFF   : oxygen diffusion coefficint ,cm2/sec.
C                CINT   : the initial concentration taken as uniform
C                         over the whole domain ,mg/cm3.
C                CONC   : the concentration at N+1th time step ,mg/cm3.
C                COLD   : the concentration at Nth time step ,mg/cm3.
C                WEIGHT : the weight gain at each time ,mg/cm2.
C                NLIM   : the maximum number of time steps taken
C                         before stopping.
C                NSTEP  : the number of time steps after which
C                         printout occurs.
C                N      : number of equations = IL - 2
C
C-------------------------------------------------------------------
C
      DIMENSION CONC(50),COLD(50)
      DIMENSION A(50),B(50),C(50),R(50),SOLN(50)
C-------------------------------------------------------------------
C

      PRINT*,'              Please enter  :
```

```
      PRINT*,'                                HEAT FLUX, QQ (W/cm2) = '
      READ(*,*)QQ
      PRINT*,'                    FAST NEUTRON FLUX, FNFLUX (n/cm2.s) = '
      READ(*,*)FNFLUX
      PRINT*,'            [LiOH] CONCENTRATION, CLOH (moles/liter) = '
      READ(*,*)CLOH
      PRINT*,'      WATER-SIDE FUEL ELEMENT SURFACE TEMP., Ts (K) = '
      READ(*,*)Ts
      PRINT*,'    MAXIMUM NO. OF TIME STEPS BEFORE STOPPING, NLIM = '
      READ(*,*)NLIM
      PRINT*,'NO. OF TIME STEPS AFTER WHICH PRINTOUT OCCURS,NSTEP = '
      READ(*,*)NSTEP
      PRINT*,'    '
      PRINT*,'-------------------------  See output file  :   ZOM.OUT
     #-----------'
      PRINT*,'    '


         TL =0.07
         TLUM=TL*1.0E4
         IL = 12
         N  = IL - 2

         STIME  = DT * NLIM
         STIMED = STIME  / (24.0*3600.0)

C
C-----------------------------------------------------------------------
C  Open the output file " ZOM.OUT "
C

      OPEN(UNIT=10,FILE='ZOM.OUT')

      WRITE(10,53)

      WRITE(10,55)

      WRITE(10,67)

      WRITE(10,68)

 53   FORMAT(18X,'ZIRCALOY OXIDATION MODEL',/)
 55   FORMAT(2X,'SOLUTION TO THE OXYGEN DIFFUSION EQUATION IN ZIRCALOY
     #FUEL CLADDING')
 67   FORMAT(/,10X,'TO CALCULATE THE OXIDE GROUTH AS FUNCTION OF TIME'
     #,/)
 68   FORMAT(/,13X,'( ONE DIMENSION,CYLINDRICAL GEOMETRY )')

      WRITE(10,56)

 56   FORMAT('-------------------------------------------------------
     #-------------------------------------------------------------')

      WRITE(10,100)DT

      WRITE(10,104)TL

      WRITE(10,111)Ts

 100  FORMAT(7X,'TIME STEP, DT =',E12.6,' sec')
```

```
      WRITE(10,224)CLOH

222   FORMAT(7X,'HEAT FLUX, QQ =',F7.2,' W/cm2')
223   FORMAT(7X,'FAST NEUTRON FLUX, FNFLUX =',E12.6,' n/cm2.sec')
224   FORMAT(7X,'[LiOH] CONCENTRATION, CLOH =',E12.6,' mole/liter')

      WRITE(10,103)STIME,STIMED

103   FORMAT(7X,'TOTAL SIMULATION TIME',' =',E12.4,2x,' sec ',
     #5X,' =',F12.5,2X,' day')

104   FORMAT(7X,'CLADDING THICKNESS, TL =',F7.4,' cm')


111   FORMAT(7X,'WATER-SIDE CLADDING TEMPERATURE, Ts =',F8.3,2X,' K')

      WRITE(10,442)

      WRITE(10,443)

      WRITE(10,444)

      WRITE(10,445)

      WRITE(10,446)

      WRITE(10,552)

      WRITE(10,553)

      WRITE(10,554)

442   FORMAT(//,7X,'THE WEIGHT GAIN AND THE OXIDE THICKNESS DEFINED AS
     *FOLLOW:')
443   FORMAT(15X,'WEXR,XEXR ==> EX-REACTOR WITH OR WITHOUT HEAT FLUX')
444   FORMAT(15X,'WLOH,XLOH ==> WITH LITHIUM HYDROXIDE')
445   FORMAT(15X,'WIRR,XIRR ==> WITH FAST NEUTRON IRRADIATION')
446   FORMAT(15X,'WINR,XINR ==> IN-REACTOR (ALL OF THE ABOVE)')
552   FORMAT(/,15X,'D         ==>THE OXYGEN DIFFUSION COEFFICIENT')
553   FORMAT(15X,'Ti        ==> OXIDE/ZIRCALOY INTERFACE TEMPERATURE')
554   FORMAT(15X,'Tc        ==> FUEL/CLAD INTERFACE TEMPERATURE'/)

      WRITE(10,56)

      ISTEP1=0
      ISTEP2=0

     TIME  =0.0
c      CONC3 =0.4387
c      CONC4 =9.3E-4
      CINT  =9.3E-4
      T=Ts
C-----------------------------------------------------------------------
C Set the initial condition:
C
      DO 10 I=1,IL
        CONC(I) = CINT
        COLD(I) = CINT
 10   CONTINUE

C-----------------------------------------------------------------------
C Set the boundary conditons:
```

```
      WRITE(10,122)

      WRITE(10,128)

      WRITE(10,56)

C-----------------------------------------------------------------------
C Solve for CONC on interior points at (N+1)th time step:
C
C     Increment the iteration counters and check for the
C     maximum limit of iterations
C
C

 20   ISTEP1=ISTEP1+1

      ISTEP2=ISTEP2+1

      TIME  =TIME  + DT

C-----------------------------------------------------------------------
C To calculate the oxide weight from emperical correlation,
C      " Hillner model "
C
C        ZRDENS : zircaloy density
C        DENS   : zircaloy oxide density
C        AZR    : zircaloy atomic weight
C        AO2    : oxygen atomic weight
C        PR     : Pilling-Bedworth ratio
C

         ZRDENS = 6.5
         AZR    = 91.22
         AO2    = 32.0
         PR     = 1.57

          TIMED  = TIME/(24.*3600.)
          TIMEDT = 6.73E-7*EXP(11975.0/T)

        IF(TIMED.LE.TIMEDT)THEN

         RKC =(6.36E11*EXP(-13636.0/T))**0.333333
         WTC  = RKC *TIMED**0.3333

         ZZ    = 1.0E-5*PR*(AZR * WTC) / (AO2 * ZRDENS)
         ZZU   = ZZ * 1.0E4

        ELSE

         RKL  =1.12E8*EXP(-12529.0/T)
         WTC  = RKL *TIMED

         ZZ   = 1.0E-5*PR*(AZR * WTC) / (AO2 * ZRDENS)
         ZZU    = ZZ * 1.0E4
         ENDIF

C
C-----------------------------------------------------------------------
C The weight gain at the transition , WTRANS (mg/dm2)
C

        WTRANS = 7.53*10.0*EXP(-553.6/T)
```

```
        DENSY = 5.82
        X =ZZU*1.0E-4
C
       DIFF =X*X*DENSY*32.0/(2.0*TIME*123.22*(CONC(1)-CONC(IL))*1.0E-3)
C
       Z=SQRT(2.0*3.8506*(DIFF/DENSY)*((CONC(1)-CONC(IL))/1000.0)*TIME)

        DX = Z /FLOAT(IL)


C
C---------------------------------------------------------------------
C    To convert the thickness from cm to  micrometer(um),
C
C         ZU=Z*1.0E4

C
C---------------------------------------------------------------------
C  To determine the effect of the heat flux on the oxide/metal
C        interface temperature"TI"
C  Tkc : thermal conductivity of the cladding "zircaloy-4",W/m.K
C  Tkx : thermal conductivity of the zircalcy oxide"ZrO2",W/m.K
C

       Tkc = 7.848+2.2E-2*T-1.676E-5*T**2.0+8.712E-9*T**3.0

       Tkkc=Tkc*1.0E-2

       Tkx = 1.9599-2.41E-4*T+6.43E-7*T**2.0-1.94E-10*T**3.0

       Tkkx=Tkx*1.0E-2
C  QQ : heat flux ,W/cm2

C        QQ = Q/AREA
C  T : oxide/metal interface temperature,K
C  TC  : fuel/clad interface temperature,K
C  CT : non-oxidized clad thickness,cm
C
        T=Ts
        Ti = T +(QQ*Z)/Tkkx
        PR = 1.57
         CT = TL - Z/PR
        TC = Ti + (QQ*CT)/Tkkc

        T=Ti
C
C---------------------------------------------------------------------
C
        IF(ISTEP1.GT.NLIM)GOTO 40
C
C
C---------------------------------------------------------------------
C Form the ridiagonal system of equations:
C
      CALL FTRDG(DX,DT,DIFF,IL,CONC,COLD,A,B,C,R)
      N=IL-2

C
C Invert the tridiagonl subroutine solver:
C
      CALL TRDG(A,B,C,R,SOLN,N)
```

```
        COLD(I)=CONC(I)
 25    CONTINUE

       DO 26 I=2,IL-1
         CONC(I)=SOLN(I)
 26    CONTINUE
C
C Impose the boundary conditons:
C
       CALL BCOND(CONC,IL,T)
C
C
       CALL TRAP(CONC,IL,DX,WEIGHT)
C
C With or without the heat flux the weight gain,WEXR (mg/dm2)
C   and the thickness,XEXR (um)

          WEXR = WEIGHT
          XEXR   = 1.0E-1 * PR *(AZR * WEXR) /( AO2 * ZRDENS)
C
C---------------------------------------------------------------------
C To calculate the lithium hydroxide [LiOH] acceleration factor,AFL:
C
C    CLOH : lithium hydroxide (mole/liter)
C
          AFL = 1.0 + 13.125 * CLOH
C
C Weight gain in the presence of LiOH ,WLOH (mg/dm2) :
C
          WLOH = WEIGHT * AFL
C
C Oxide thickness XLOH ,um :
C
          XLOH = 1.0E-1 *PR*(AZR * WLOH )/( AO2 * ZRDENS)
C
C---------------------------------------------------------------------
C To calculate the fast neutron enhancement factor,AFR
C
C      FNFLUX : fast neutron flux ,(n/cm2 sec)
C      WIRR   : weight gain with irradiation (mg/dm2) and
C      XIRR   : oxide thickness(um)
C      U,AM and CO are constants
C
              U  = 2.59E8
              AM = 7.46E-15
              CO = 8.04E7
         IF((WEXR.GE.WTRANS).and.(FNFLUX.GE.1.0E12))THEN
              AFR = 1.0 + ( U / CO ) * (AM*FNFLUX)**0.24
              WIRR= WEXR*AFR
          ELSE
              AFR = 1.0
              WIRR=WEXR*AFR

         ENDIF
C             WIRR = WEXR * AFR

              XIRR = 1.0E-1 * PR * ( AZR * WIRR) / (AO2 * ZRDENS)
C
C---------------------------------------------------------------------
C The in-reactor weight gain,WINR(mg/dm2) and thickness,XINR(um)
C  due to the lithium hydrooxide and fast neutron flux:
C
```

```
C
            XXX = PR * TLUM

           IF(XINR.GT.XXX)GOTO 199

C
C-----------------------------------------------------------------
C Output the results:
C
         IF(ISTEP2.EQ.NSTEP)THEN


 122   FORMAT(/,T3,'TIME (day)',T22,' WEIGHT GAIN   (mg/dm2) ',
     *T58,'OXIDE THICKNESS  (micro m) ',T89,'TEMPERATURE (K)  ',
     *' D (cm2/sec)')
 128   FORMAT(T18,'WEXR',5X,'WLOH',5X,'WIRR',5X,'WINR',
     *T57,'XEXR',4X,'XLOH',4X,'XIRR',4X,'XINR',T92,'Ti',6X,'Tc')
       WRITE(10,133)TIMED,WEXR,WLOH,WIRR,WINR,XEXR,XLOH,XIRR,XINR,
     *T,TC,DIFF

 133   FORMAT(F12.5,1X,4(1X,F8.2),T53,4(1X,F7.3),T89,F7.2,1X,F7.2,1X,
     #E12.4)

       ISTEP2=0

       GOTO 20
         ENDIF
       GOTO 20

 199   WRITE(10,299)

 299   FORMAT(//,'-----*+([[ SORY ]])+*-----   the  cladding (zircaloy)
     *has turned completely to oxide   -----*+([[ SORY ]])+*-----')
 40    CLOSE(UNIT=10)
       STOP
       END

C-----------------------------------------------------------------
C
       SUBROUTINE FTRDG(DX,DT,DIFF,IL,CONC,COLD,A,B,C,R)
C
C This subroutine forms the tridiagonal matix.
C
C The generic form of the equation is:
C
C         A*CONC(I-1) + B*CONC(I) + C*CONC(I+1) = R
C
C
       DIMENSION CONC(50),COLD(50),A(50),B(50),C(50),R(50)
C

       RO = 0.48
       N=IL-2
        DD = (DIFF*DT) / DX**2
        EE = (DIFF*DT) / 2.0*RO*DX
        A(1)=0.0
       DO 10 I=2,N
       A(I) =-(DD-EE)
 10    CONTINUE
       C(N)=0.0
```

```
      DO 19 I=1,N
      B(I) =1.0 + (2.0*DD)
 19   CONTINUE

      DO 20 I=1,N
      R(I) =COLD(I)

C
C Incorporate the appropriate boundary conditions:
C
C  Left boundary:
C

      IF(I.EQ.1)R(I)=R(I)+(( DD-EE )*CONC(1))
C
C  Right boundary:
C

      IF(I.EQ.N)THEN
      R(I)=R(I)+(( DD-EE )*CONC(IL))

      ENDIF


 20   CONTINUE
      RETURN
      END


C---------------------------------------------------------------------
C This subroutines inverts a tridiagonal matrix by THOMAS algorithm.
C
C Solution is returned in the array called 'SOLN'.
C

      SUBROUTINE TRDG(A,B,C,R,SOLN,N)

      DIMENSION A(50),B(50),C(50),R(50),SOLN(50),BN(50)

      DO 5 I=1,N
      BN(I)=B(I)
 5    CONTINUE
      DO 6 I=2,N
      D=A(I)/BN(I-1)
      BN(I)=BN(I)-C(I-1)*D
      R(I)=R(I)-R(I-1)*D
 6    CONTINUE
C
C Back substituation
C
      SOLN(N+1)=R(N)/BN(N)

      DO 30 I=1,N-1
      J=N-I
      SOLN(J+1)=(R(J)-C(J)*SOLN(J+2))/BN(J)

 30   CONTINUE
      RETURN
      END

C---------------------------------------------------------------------
C Boundary conditions subroutine:
```

```
C Left  boundary:
C
       CONC(1) =1526.0

C
C Right boundary:
C

      CONC(IL)= (1.5494 - 9.7E-5*T) * 1000.0
      RETURN
      END

C---------------------------------------------------------------------
C  To calculate the total concentration of the oxide (mg/cm2):
C
      SUBROUTINE TRAP(CONC,IL,DX,WEIGHT)
      DIMENSION CONC(50)

      SUM = CONC(1)
      DO 17 I=2,IL-1
      SUM = SUM + 2.0 * CONC(I)
 17   CONTINUE
      WEIGH = ( DX / 2.0 ) * ( SUM + CONC(IL) )
C
C  To convert the weight from (mg/cm2) to (mg/dm2)
C
      WEIGHT = WEIGH *100.0

      RETURN
      END

C---------------------------------------------------------------------
```

Appendix B: Sample Output (ZOM.OUT)

ZIRCALOY OXIDATION MODEL

SOLUTION TO THE OXYGEN DIFFUSION EQUATION IN ZIRCALOY FUEL CLADDING

TO CALCULATE THE OXIDE GROUTH AS FUNCTION OF TIME

(ONE DIMENSION,CYLINDRICAL GEOMETRY)

TIME STEP, DT = 86.0 sec
CLADDING THICKNESS, TL = 0.0700 cm
WATER-SIDE CLADDING TEMPERATURE, Ts = 633.000 K
HEAT FLUX, QQ = 80.00 W/cm2
FAST NEUTRON FLUX, FNFLUX =0.200000E+13 n/cm2.sec
[LiOH] CONCENTRATION, CLOH =0.100000E-02 mole/liter
TOTAL SIMULATION TIME = 0.8640E+08 sec = 1000.00000 day

THE WEIGHT GAIN AND THE OXIDE THICKNESS DEFINED AS FOLLOW:
WEXR,XEXR => EX-REACTOR WITH OR WITHOUT HEAT FLUX
WLOH,XLOH => WITH LITHIUM HYDROXIDE
WIRR,XIRR => WITH FAST NEUTRON IRRADIATION
WINR,XINR => IN-REACTOR (ALL OF THE ABOVE)

D =>THE OXYGEN DIFFUSION COEFFICIENT
Ti => OXIDE/ZIRCALOY INTERFACE TEMPERATURE
Tc => FUEL/CLAD INTERFACE TEMPERATURE

TIME (day)	WEIGHT GAIN (mg/dm2)				OXIDE THICKNESS (micro m)				TEMPERATURE (K)		D (cm2/sec)
	WEXR	WLOH	WIRR	WINR	XEXR	XLOH	XIRR	XINR	Ti	Tc	
10.00000	13.47	13.65	13.47	13.65	0.928	0.940	0.928	0.940	633.39	665.78	0.2186E-12
20.00000	16.99	17.22	16.99	17.22	1.170	1.185	1.170	1.185	633.49	665.87	0.1739E-12
30.00000	19.47	19.73	19.47	19.73	1.341	1.358	1.341	1.358	633.56	665.94	0.1521E-12
40.00000	21.45	21.73	21.45	21.73	1.477	1.496	1.477	1.496	633.62	665.99	0.1384E-12
50.00000	23.12	23.42	23.12	23.42	1.592	1.612	1.592	1.612	633.66	666.03	0.1286E-12
60.00000	24.58	24.90	24.58	24.90	1.692	1.714	1.692	1.714	633.71	666.07	0.1211E-12
70.00000	25.89	26.23	25.89	26.23	1.782	1.806	1.782	1.806	633.74	666.10	0.1151E-12
80.00000	27.08	27.43	27.08	27.43	1.864	1.889	1.864	1.889	633.78	666.13	0.1102E-12
90.00000	28.17	28.54	28.17	28.54	1.940	1.965	1.940	1.965	633.81	666.16	0.1060E-12
100.00000	29.19	29.58	29.19	29.58	2.010	2.036	2.010	2.036	633.84	666.19	0.1024E-12
110.00000	30.55	30.95	30.55	30.95	2.103	2.131	2.103	2.131	633.88	666.22	0.1019E-12
120.00000	33.41	33.85	72.65	73.60	2.301	2.331	5.002	5.068	633.96	666.30	0.1117E-12
130.00000	36.29	36.77	78.91	79.95	2.499	2.532	5.433	5.505	634.04	666.37	0.1217E-12
140.00000	39.19	39.70	85.21	86.32	2.698	2.734	5.867	5.944	634.12	666.45	0.1317E-12
150.00000	42.10	42.65	91.54	92.74	2.899	2.937	6.303	6.385	634.21	666.52	0.1418E-12
160.00000	45.03	45.62	97.90	99.19	3.100	3.141	6.741	6.829	634.29	666.60	0.1520E-12
170.00000	47.97	48.60	104.30	105.67	3.303	3.346	7.182	7.276	634.38	666.67	0.1623E-12
180.00000	50.93	51.60	110.74	112.19	3.507	3.553	7.625	7.725	634.46	666.75	0.1727E-12
190.00000	53.91	54.62	117.21	118.75	3.712	3.760	8.070	8.176	634.55	666.83	0.1832E-12
200.00000	56.90	57.65	123.71	125.34	3.918	3.969	8.518	8.630	634.63	666.91	0.1939E-12
210.00000	59.91	60.70	130.26	131.97	4.125	4.179	8.969	9.086	634.72	666.98	0.2046E-12
220.00000	62.94	63.76	136.84	138.63	4.333	4.390	9.422	9.545	634.80	667.06	0.2155E-12
230.00000	65.98	66.85	143.46	145.34	4.543	4.603	9.877	10.007	634.89	667.14	0.2264E-12
240.00000	69.04	69.95	150.11	152.08	4.754	4.816	10.336	10.471	634.98	667.22	0.2375E-12
250.00000	72.12	73.07	156.80	158.86	4.966	5.031	10.797	10.938	635.07	667.30	0.2487E-12
260.00000	75.22	76.20	163.54	165.68	5.179	5.247	11.260	11.408	635.16	667.38	0.2600E-12
270.00000	78.33	79.36	170.31	172.54	5.393	5.464	11.726	11.880	635.25	667.46	0.2715E-12
280.00000	81.46	82.53	177.12	179.44	5.609	5.683	12.195	12.355	635.33	667.54	0.2830E-12
290.00000	84.62	85.73	183.97	186.39	5.826	5.903	12.667	12.833	635.42	667.62	0.2947E-12
300.00000	87.78	88.94	190.86	193.37	6.044	6.124	13.142	13.314	635.52	667.71	0.3065E-12

310.00000	90.97	92.17	197.80	200.39	6.264	6.346	13.619	13.798	635.61	667.79	0.3185E-12
320.00000	94.13	95.42	204.77	207.46	6.485	6.570	14.099	14.284	635.70	667.87	0.3305E-12
330.00000	97.41	98.69	211.79	214.57	6.707	6.795	14.582	14.774	635.79	667.95	0.3427E-12
340.00000	100.66	101.98	218.85	221.72	6.931	7.022	15.069	15.266	635.88	668.04	0.3551E-12
350.00000	103.92	105.29	225.95	228.92	7.156	7.249	15.558	15.762	635.98	668.12	0.3676E-12
360.00000	107.21	108.62	233.10	236.16	7.382	7.479	16.050	16.260	636.07	668.21	0.3802E-12
370.00000	110.52	111.97	240.29	243.45	7.610	7.710	16.545	16.762	636.17	668.29	0.3929E-12
380.00000	113.85	115.34	247.53	250.78	7.839	7.942	17.043	17.267	636.26	668.38	0.4058E-12
390.00000	117.20	118.74	254.81	258.16	8.069	8.175	17.545	17.775	636.36	668.47	0.4189E-12
400.00000	120.57	122.15	262.14	265.58	8.302	8.410	18.049	18.286	636.45	668.55	0.4321E-12
410.00000	123.96	125.59	269.52	273.05	8.535	8.647	18.557	18.801	636.55	668.64	0.4454E-12
420.00000	127.37	129.05	276.94	280.57	8.770	8.885	19.068	19.319	636.65	668.73	0.4589E-12
430.00000	130.81	132.53	284.41	288.14	9.007	9.125	19.583	19.840	636.74	668.82	0.4726E-12
440.00000	134.27	136.03	291.93	295.76	9.245	9.366	20.101	20.364	636.84	668.91	0.4864E-12
450.00000	137.75	139.56	299.50	303.43	9.485	9.609	20.622	20.892	636.94	669.00	0.5004E-12
460.00000	141.26	143.11	307.12	311.15	9.726	9.854	21.146	21.424	637.04	669.09	0.5146E-12
470.00000	144.78	146.68	314.79	318.92	9.969	10.100	21.675	21.959	637.14	669.18	0.5289E-12
480.00000	148.34	150.28	322.52	326.75	10.213	10.348	22.206	22.498	637.24	669.27	0.5434E-12
490.00000	151.91	153.91	330.29	334.63	10.460	10.597	22.742	23.040	637.35	669.36	0.5581E-12
500.00000	155.51	157.55	338.12	342.56	10.708	10.848	23.281	23.586	637.45	669.46	0.5729E-12
510.00000	159.14	161.23	346.00	350.54	10.957	11.101	23.823	24.136	637.55	669.55	0.5880E-12
520.00000	162.79	164.93	353.94	358.58	11.209	11.356	24.370	24.690	637.66	669.64	0.6032E-12
530.00000	166.47	168.65	361.93	366.68	11.462	11.612	24.920	25.247	637.76	669.74	0.6186E-12
540.00000	170.17	172.40	369.98	374.84	11.717	11.870	25.475	25.809	637.87	669.83	0.6342E-12
550.00000	173.90	176.18	378.09	383.05	11.973	12.131	26.033	26.374	637.97	669.93	0.6501E-12
560.00000	177.65	179.98	386.25	391.32	12.232	12.393	26.595	26.944	638.08	670.03	0.6661E-12
570.00000	181.43	183.82	394.48	399.65	12.492	12.656	27.161	27.518	638.19	670.12	0.6823E-12
580.00000	185.24	187.68	402.76	408.05	12.755	12.922	27.732	28.096	638.30	670.22	0.6987E-12
590.00000	189.08	191.56	411.11	416.50	13.019	13.190	28.306	28.678	638.41	670.32	0.7153E-12
600.00000	192.95	195.48	419.51	425.02	13.285	13.460	28.885	29.264	638.52	670.42	0.7322E-12
610.00000	196.85	199.43	427.98	433.60	13.553	13.731	29.468	29.855	638.63	670.52	0.7493E-12
620.00000	200.77	203.41	436.52	442.25	13.824	14.005	30.056	30.450	638.74	670.62	0.7666E-12
630.00000	204.73	207.41	445.12	450.96	14.096	14.281	30.648	31.050	638.85	670.72	0.7842E-12
640.00000	208.71	211.45	453.78	459.74	14.371	14.559	31.245	31.655	638.97	670.83	0.8019E-12
650.00000	212.73	215.52	462.52	468.59	14.647	14.839	31.846	32.264	639.08	670.93	0.8200E-12
660.00000	216.78	219.62	471.32	477.50	14.926	15.122	32.452	32.878	639.19	671.04	0.8382E-12
670.00000	220.86	223.75	480.19	486.49	15.207	15.406	33.063	33.497	639.31	671.14	0.8568E-12
680.00000	224.97	227.92	489.13	495.55	15.490	15.693	33.678	34.120	639.43	671.25	0.8756E-12
690.00000	229.11	232.12	498.14	504.68	15.775	15.982	34.299	34.749	639.55	671.35	0.8946E-12
700.00000	233.29	236.36	507.23	513.89	16.063	16.274	34.925	35.383	639.66	671.46	0.9139E-12
710.00000	237.51	240.63	516.39	523.17	16.353	16.568	35.556	36.022	639.78	671.57	0.9335E-12
720.00000	241.76	244.93	525.63	532.53	16.646	16.864	36.192	36.667	639.91	671.68	0.9534E-12
730.00000	246.04	249.27	534.95	541.97	16.941	17.163	36.833	37.316	640.03	671.79	0.9736E-12
740.00000	250.36	253.65	544.34	551.49	17.238	17.465	37.480	37.972	640.15	671.90	0.9941E-12
750.00000	254.72	258.06	553.82	561.09	17.538	17.769	38.132	38.633	640.27	672.01	0.1015E-11
760.00000	259.12	262.52	563.37	570.77	17.841	18.075	38.790	39.299	640.40	672.13	0.1036E-11
770.00000	263.55	267.01	573.01	580.53	18.146	18.384	39.454	39.972	640.53	672.24	0.1057E-11
780.00000	268.02	271.54	582.74	590.39	18.454	18.697	40.124	40.650	640.65	672.35	0.1079E-11
790.00000	272.54	276.11	592.55	600.33	18.765	19.011	40.799	41.335	640.78	672.47	0.1101E-11
800.00000	277.09	280.73	602.45	610.36	19.079	19.329	41.481	42.025	640.91	672.59	0.1124E-11
810.00000	281.68	285.38	612.44	620.48	19.395	19.650	42.169	42.722	641.04	672.71	0.1146E-11
820.00000	286.32	290.08	622.53	630.70	19.714	19.973	42.863	43.426	641.17	672.83	0.1169E-11
830.00000	291.00	294.82	632.70	641.01	20.037	20.300	43.564	44.136	641.31	672.95	0.1193E-11
840.00000	295.73	299.61	642.97	651.41	20.362	20.629	44.271	44.852	641.44	673.07	0.1217E-11
850.00000	300.50	304.44	653.35	661.92	20.690	20.962	44.985	45.576	641.58	673.19	0.1241E-11
860.00000	305.31	309.32	663.82	672.53	21.022	21.298	45.706	46.306	641.71	673.31	0.1266E-11
870.00000	310.18	314.25	674.39	683.24	21.357	21.637	46.434	47.044	641.85	673.44	0.1291E-11
880.00000	315.09	319.22	685.07	694.06	21.695	21.980	47.169	47.789	641.99	673.57	0.1316E-11
890.00000	320.05	324.25	695.85	704.99	22.036	22.326	47.912	48.541	642.13	673.69	0.1342E-11
900.00000	325.06	329.33	706.75	716.02	22.381	22.675	48.662	49.301	642.27	673.82	0.1369E-11
910.00000	330.12	334.45	717.75	727.17	22.730	23.028	49.420	50.069	642.42	673.95	0.1395E-11
920.00000	335.24	339.64	728.87	738.44	23.082	23.385	50.186	50.844	642.56	674.08	0.1423E-11
930.00000	340.40	344.87	740.11	749.82	23.438	23.746	50.959	51.628	642.71	674.22	0.1451E-11

940.00000	345.63	350.16	751.47	761.33	23.798	24.110	51.741	52.420	642.86	674.35	0.1479E-11
950.00000	350.91	355.51	762.95	772.96	24.161	24.478	52.532	53.221	643.01	674.49	0.1508E-11
960.00000	356.25	360.92	774.55	784.72	24.529	24.851	53.331	54.031	643.16	674.62	0.1537E-11
970.00000	361.64	366.39	786.29	796.61	24.900	25.227	54.139	54.849	643.31	674.76	0.1567E-11
980.00000	367.10	371.92	798.16	808.63	25.276	25.608	54.956	55.677	643.47	674.90	0.1597E-11
990.00000	372.62	377.51	810.16	820.79	25.656	25.993	55.782	56.515	643.62	675.05	0.1628E-11
1000.00000	378.21	383.17	822.30	833.10	26.041	26.383	56.618	57.362	643.78	675.19	0.1660E-11